Glass fibre concrete: experimental investigation and predictive modeling using advanced machine learning with an interactive online interface

Construction and Building Materials 472 (2025) 140951

Contents lists available at ScienceDirect

Construction and Building Materials

journal homepage: www.elsevier.com/locate/conbuildmat

Glass fibre concrete: Experimental investigation and predictive modeling using advanced machine learning with an interactive online interface

Mohamed Rabie *, Ibrahim G. Shaaban

School of Computing and Engineering, University of West London, St Mary's Road, Ealing, London W5 5RF, UK

ARTICLE INFO

Keywords:
Glass fibre concrete
Machine learning
Hyperparameter optimization
Compressive strength
Split tensile strength
Durability
Online user-friendly interface

ABSTRACT

This study investigates the mechanical properties of glass fibre concrete (GFC) through experimental and predictive analysis using advanced machine learning (ML) techniques. The experimental work focuses on the mechanical and durability characteristics of GFC. The data obtained in the experimental testing were added to the dataset collected from the literature for the application of machine learning algorithms. The dataset contains 108 compressive strength and 87 split tensile strength data points that evaluated vital factors, including fly ash, cement, aggregates, water, fibre content, superplasticizer, fibre length, fibre diameter, and micro-silica. Optuna, a state-of-the-art hyperparameter optimization library utilizing deep learning, was employed to determine the optimal hyperparameters for each model. The best hyperparameters were selected based on the highest average performance from 5-fold cross-validation. Experimental results showed significant influences of fibre content on GFC mechanical and durability characteristics. The Gradient Tree Boosting Regression (GTBR) model was identified as the optimal model for predicting the compressive and split tensile strength of GFC. The model demonstrated high predictive accuracy for both compressive and split tensile strengths, with R^2 values of 0.968 and 0.954, respectively. Shapley Additive exPlanations (SHAP) analysis emphasized the significant impact of fine aggregate, cement, and the amount of glass fibre on both compressive and split tensile strengths, providing valuable insights into the contribution of each feature and enhancing the explainability of the optimum ML model. Finally, a user-friendly online interface was developed, allowing users to predict GFC properties based on the trained GTBR model. This tool, featuring interactive sliders for input variables, ensures precise predictions within the collected data range.

1. Introduction

Fibre Reinforced Concrete (FRC) is widely used in numerous applications, including tunnel linings, railway slabs, concrete barriers, and ground slabs. Plain concrete, while strong in compression, is inherently brittle and has low tensile strength [1–3]. The addition of fibres significantly enhances its tensile properties by bridging cracks, thereby preventing their propagation and improving both strength and post-cracking behaviour [4]. Normal Strength Concrete (NSC), commonly used in construction, is prone to issues such as plastic and drying shrinkage cracking. Incorporating fibres can effectively reduce these shrinkage cracks and enhance the mechanical properties of concrete [5].

Recent research has investigated various types of fibre in FRC, including metal, synthetic, and mineral fibre, each offering unique properties [6]. Several studies have shown that the compressive strength of concrete increases with higher fibre dosage, especially when using steel, glass, and polyvinyl alcohol fibre [7–9]. However, some research indicates that glass fibre do not significantly affect compressive strength [10,11]. While it is well established that fibers improve the tensile properties of concrete, the effect on compressive strength remains inconsistent across studies. Research indicates that the loss of compressive strength depends on fiber size, surface texture, and dispersion within the matrix, which influence porosity and the bond strength at the fiber-matrix interface [12]. Larger fiber diameters and smooth fiber surfaces often reduce the bond strength, leading to lower compressive strength, whereas rougher textures improve mechanical interlocking and stress transfer [10]. Furthermore, improper dispersion of fibers can create localized weak zones with increased porosity, negatively impacting mechanical performance [13].

Despite extensive research on the effects of fibres on compressive properties, there remains a notable gap in studies specifically examining

* Correspondence to: London W5 5RF, UK.
E-mail address: mohamed.rabie@uwl.ac.uk (M. Rabie).

https://doi.org/10.1016/j.conbuildmat.2025.140951
Received 25 June 2024; Received in revised form 26 February 2025; Accepted 17 March 2025
Available online 23 March 2025

specific volume fractions, and lack of theoretical models to predict the mechanical properties of GFC. Given the complexities of traditional methods for determining the mechanical properties of glass fibre concrete, there is increasing interest in utilizing innovative approaches, particularly those involving advanced machine learning (ML). Few studies have investigated the application of advanced ML techniques, such as ensemble ML algorithms, to estimate the mechanical properties of glass fibre concrete [14,15]. Historically, research has predominantly used traditional machine learning models and basic artificial neural networks to predict properties, such as compressive and tensile strengths [16–18]. While these conventional methods offer simplicity and interpretability, they often face limitations in predictive accuracy, especially when addressing the complex, non-linear interactions characteristic of fibrous concrete materials. This gap highlights the need for more sophisticated ML approaches to enhance prediction capabilities and optimize the performance of glass fibre concrete.

This study aims to evaluate the mechanical and durability properties of Glass Fibre Reinforced Concrete (GFC) through experimental analysis and machine learning (ML)-based predictive modeling. The research specifically investigates how fibre parameters (content, length, and diameter), cementitious material proportions (cement, fly ash, microsilica), and mix properties (water-cement ratio, superplasticizer) influence compressive strength, split tensile strength. Furthermore, the study integrates advanced machine learning models to predict GFC properties with high accuracy and provide an explainable feature importance ranking through SHAP analysis. This approach enables a comprehensive understanding of the relationships between material composition and concrete performance, contributing to optimized mix designs for structural applications. Fig. 1 illustrates the flowchart for the ML framework applied in this research.

2. Research significance

Understanding and predicting the mechanical properties of glass fibre concrete (GFC) is essential in civil engineering and construction to ensure the structural integrity and durability of buildings and infrastructure. Despite its importance, there is a lack of widely used, data-driven methods for estimating the compressive and split tensile strengths of GFC. This research addresses this gap by leveraging advanced machine learning (ML) models to accurately predict these properties. Additionally, a user-friendly online interface has been developed to make these ML predictions accessible to academics and professionals.

The main goals of this research are:

- Identify the optimal mix design for GFC that enhances both mechanical properties (compressive and split tensile strength) and durability.
- Develop predictive ML models capable of accurately estimating GFC properties based on material composition.
- Analyze the contribution of individual input variables (fiber content, cement, aggregates, etc.) to GFC strength using SHAP analysis.
- Provide an accessible online tool that allows practitioners to predict the mechanical properties of GFC for specific mix compositions.

3. Materials and methods

3.1. Materials

Ordinary Portland cement (OPC) ASTM Type I was used in this study. Natural Coarse aggregates with a maximum size of 10 mm and retained on 4 mm sieve. Fine aggregate, natural sand, with a maximum size of 2.36 mm and below was considered in this study. Fine aggregate was dried in the open air before usage. All the materials were sourced from Travis Perkins [19]. Potable tap water is used for mixing and curing of the test specimens.

Commercially available Alkali Resistant Glass Fibre (GF) from Oscrete Construction Products, was used in this research its general properties are listed in Table 1.

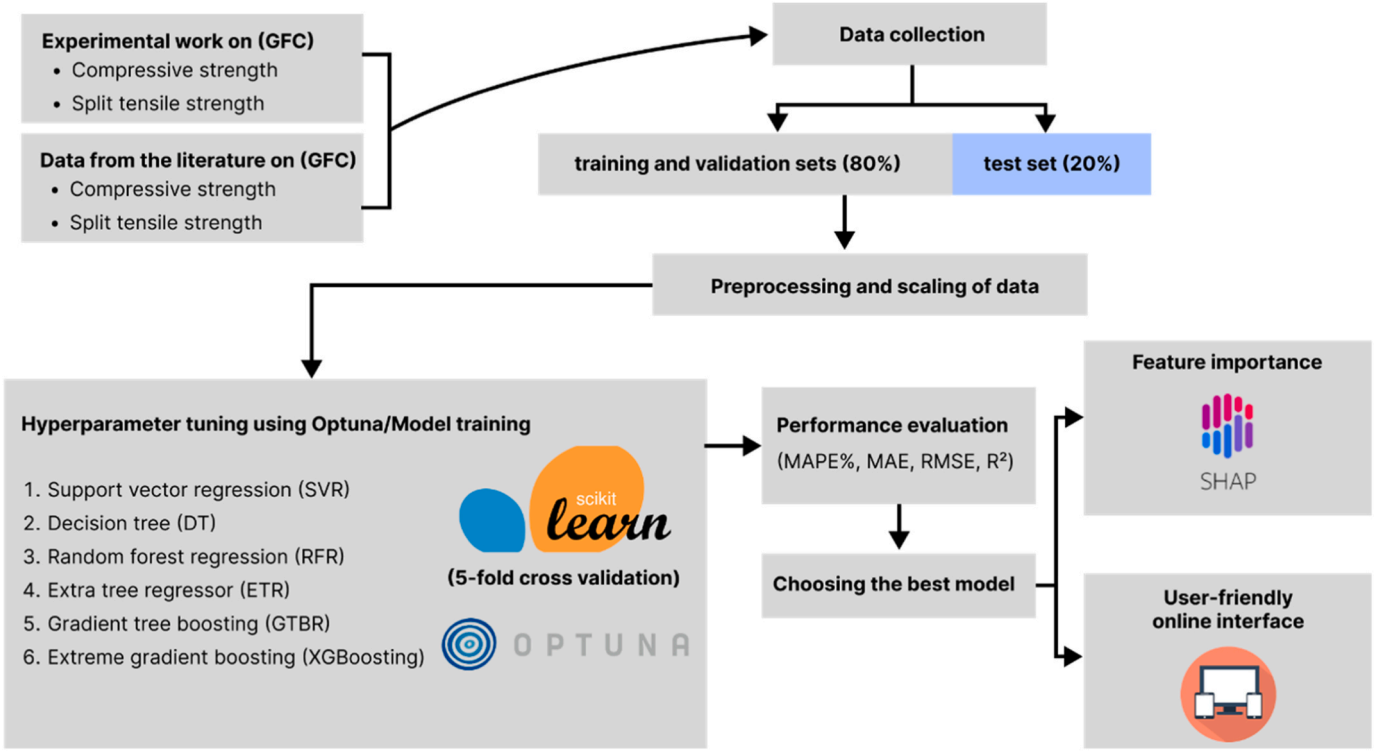

Fig. 1. Flowchart of the ML process with the user-friendly interface.

Table 1
Fibre properties.

Specific Gravity (g/cm^3)	Fibre Length (mm)	Modulus of Elasticity (GPa)	Tensile Strength (MPa)	Softening Point (°C)
2.68	12	72	1700	860

3.2. Mix proportions

Concrete mix design of characteristic strength 30 MPa using Ordinary Portland Cement Type I was considered in this study. As the primary function of Fiber Reinforced Concrete (FRC) is not to maximize compressive strength but to enhance the tensile strength-to-compressive strength ratio and improve ductility. Prior research has shown that higher compressive strength may overshadow the relative improvements in tensile properties, making it more challenging to isolate fiber effects [20]. Additionally, many real-world applications of GFC—such as overlays, industrial floors, and repair materials—require moderate compressive strengths while prioritizing improved tensile and post-cracking behaviour [12]. Total of four mixes were prepared, the control mix is made of cement, water, coarse aggregates, and fine aggregates. The water-cement ratio was maintained at 0.4 for all design mixes in this investigation. Three percentages of glass fibre were examined: G1 with 0.75 % by cement weight (equivalent to a 0.12 % V_f), G2 with 1.32 % by cement weight (0.22 % V_f), and G3 with 2.63 % by cement weight (0.43 % V_f). These specific percentages were chosen because there were no previous studies in the literature that investigated these particular values, and it will be used in the training of the proposed machine learning model. The details of the mix design are depicted in Table 2.

3.3. Experimental procedure

The mixing process began by thoroughly combining the coarse and fine aggregates. Glass fibres were then gradually incorporated into this mixture, ensuring a homogeneous blend. Following this, cement was added to the mixer, and water was introduced incrementally. Once a uniform and consistent mix was achieved, the slump test was performed to evaluate the workability of the concrete as shown in Fig. 2.

3.3.1. Fresh properties

The slump test conducted in this study adhered to the standards specified in BS EN 12350–2:2009 [21]. After placing the concrete mixes in the moulds, they were vibrated to facilitate the removal of air bubbles and to ensure the liquefaction of mixtures with lower water content. The specimens were then kept in the steel moulds for the first 24 hours under lab conditions.

3.3.2. Hardened properties

The compressive strength test conducted in this study followed the guidelines of BS 1881: Part 116:1983 [22]. Concrete cube samples, each measuring 150 mm × 150 mm × 150 mm, were used. Six specimens were prepared for testing at 7, and 28 days. After 24 hours of casting, the concrete specimens were demoulded and placed in a curing tank for water curing. The compressive strength tests were performed at 7 days and 28 days post-curing.

The splitting tensile strength test was conducted according to ASTM C 496 [23], using a Universal Testing Machine with a capacity of 3000 kN. Cylindrical samples, 150 mm in diameter and 300 mm in height, were tested after 28 days of water curing.

Table 2
Mix design proportions.

Mix ID	Cement (Kg/m^3)	Fine aggregate (Kg/m^3)	Coarse aggregate (Kg/m^3)	Water (Kg/m^3)	Fibre amount (Kg/ m^3)
Control	440	752	1158	176	0
G1	440	752	1158	176	3.3
G2	440	752	1158	176	5.808
G3	440	752	1158	176	11.572

3.3.3. Rate of water absorption

Measurements of capillary absorption were carried out using the cubes after oven drying in the oven for 24 hours at 110 °C and after cooling in the laboratory temperature then rested on rods in water containers to allow free access of water to the inflow surface as shown in Fig. 3. The water level was maintained to remain at no more than about 5 mm above the base of the specimens. The lower areas on the sides of the specimens were coated with grease to achieve unidirectional flow. The cumulative water absorbed was recorded at different time intervals of up to two hours by weighing the specimen after removing the surface water using a dampened tissue.

3.3.4. Bulk density

To determine the bulk density three concrete cubes, each with dimensions of 150 mm, were prepared for each mix design. These cubes were subjected to oven drying at a temperature of 110°C for a duration of 24 hours to ensure complete removal of moisture. Then the specimens were allowed to cool to ambient temperature for a period of 2 hours and the dry weight of each specimen was recorded. The bulk density was calculated by dividing the oven-dry weight of each cube by its volume. The average bulk density for each mix design was then determined by averaging the densities of the three specimens.

3.3.5. Moisture content

Moisture content is a key factor in concrete's durability and strength. To measure it, samples were removed from the curing tank and surface-dried with a cloth. Each sample was then weighed to obtain the wet weight. By comparing this wet weight with the dry weight recorded earlier, the moisture content was calculated.

3.4. Machine learning framework

3.4.1. Data description

To conduct this study, a comprehensive dataset comprising 108 data points for compressive strength and 87 data points for split tensile strength was gathered from 26 journal articles and the experimental work conducted in this study [5,24–48]. The full dataset is detailed in the appendix section. This dataset encompasses key factors influencing the mechanical properties of glass fibre concrete. The factors included in this study are fly ash content, cement content, fine and coarse aggregate contents, water content, amount of fibre, superplasticizer (SP) content, fibre length, fibre diameter, and microsilica content. These variables were used to evaluate their impact on both compressive and split tensile strengths of glass fibre concrete using different ML algorithms. Table 3 provides a detailed overview of the dataset's descriptive statistics and variable nomenclature.

3.5. Pre-processing of data

3.5.1. Correlation matrix

A correlation matrix was used to identify linear associations between dataset features, as shown in Fig. 4. It quantifies relationships between input variables and the output variable, with values ranging from −1 (perfect inverse correlation) to 1 (perfect direct correlation).

The correlation matrices for compressive strength (CS) shown in Fig. 4a and split tensile strength (ST) shown in Fig. 4b of glass fibre concrete highlight several important factors. For compressive strength, fly ash (0.50) and superplasticizer (SP) (0.47) show moderate positive correlations, indicating their significant influence. Conversely, microsilica exhibits a weak negative correlation (-0.071). For split tensile

(a) (b)

Fig. 2. Mixing of concrete specimens; (a) Adding GF to the mix; (b) Concrete samples in moulds.

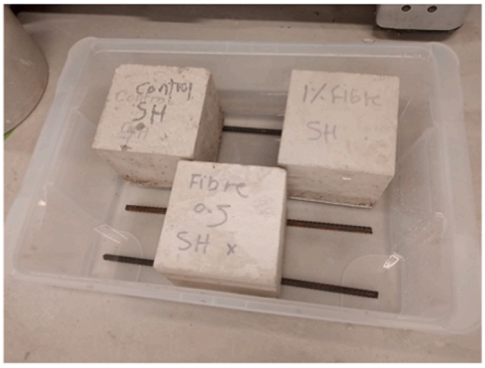

Fig. 3. Rate of water absorption with the cubes in the capillary tray.

Table 3
Descriptive statistics of the dataset.

Parameters	Mean	Standard deviation	Minimum	Maximum
MicroSilica (Kg/m^3)	14.880	29.550	0	132
Fly Ash (Kg/m^3)	33.141	55.494	0	137.5
fine aggregate (Kg/m^3)	786.898	107.986	600	1100
coarse aggregate (Kg/m^3)	905.322	294.943	0	1333
Cement (Kg/m^3)	432.788	124.099	280	940
Water (Kg/m^3)	180.281	34.545	129	319.6
Amount of fibre (Kg/m^3)	11.970	13.775	0	53.6
SP ((Kg/m^3)	5.684	6.398	0	26.37
Diameter (μm)	26.685	87.431	0	540
Length (mm)	14.093	12.168	0	50
Compressive strength (MPa)	52.135	14.623	23.2	84.079
Split-tensile strength (MPa)	4.544	1.465	2	10.010

strength, microsilica (0.26), amount of fibre (0.23), and superplasticizer (SP) (0.22) show weak positive correlations, suggesting their positive impact. Fly ash, on the other hand, shows a weak negative correlation (-0.097). These factors are crucial in understanding the mechanical properties of glass fibre concrete and guide further optimization of concrete mix designs using the proposed ML algorithms.

3.5.2. Data visualization using pair plots

Scatter plots were created to visualize the pairwise relationships among the dataset's features for the compressive and split tensile strengths of glass fibre concrete (GFC) using the Seaborn library in Python [49], as depicted in Figure A1 and Figure A2. These plots provide a comprehensive view of the distributions and interactions between variables, offering initial insights into potential outliers and the overall data structure. Both the correlation matrix and pair plots are crucial for developing hypotheses about feature interactions and identifying various trends within the data.

3.6. Proposed ML models

This section offers a summary of the ML models utilized in the research. Six ML models were evaluated with the objective of formulating a robust and accurate prediction model for the compressive and split tensile strength of glass fibre concrete, as discussed below.

3.6.1. Support vector regression

Support Vector Regression (SVR) is a machine learning algorithm used to predict continuous target values by mapping data into a higher-dimensional space using a kernel function. In this space, a hyperplane is identified that minimizes the error between predicted and actual values within a predefined margin of tolerance, known as the epsilon (ε)-tube. This technique optimizes the tube to best fit the data for accurate predictions. [50–55].

SVR employs four types of kernel functions:

- Linear Kernel: Computes the dot product of two input vectors, suitable for linearly separable data.
- Polynomial Kernel: Computes the dot product raised to a power, suitable for non-linearly separable data. Higher degrees increase complexity and risk of overfitting.
- Hyperbolic Tangent Kernel: A non-linear function similar to the sigmoid function, less prone to overfitting compared to the polynomial kernel.
- Radial Basis Function (RBF) Kernel: Based on the Gaussian distribution, this non-linear function is robust against overfitting and suitable for non-linearly separable data. The width of the kernel affects the smoothness of the resulting curve.

Hyperparameters for all four kernels were optimized to ensure the best predictive performance of the SVR model.

3.6.2. Decision tree

The Decision Tree (DT) is a non-parametric supervised machine learning technique with a flowchart-like structure. Predictions are made by following paths from the root to the leaf nodes, where each internal node represents a test, and each leaf node represents the test's outcome. DTs can be used for both classification and regression tasks. For regression, the tree splits the data into terminal nodes and establishes a regression model within each node, using the feature that provides the most significant information gain [56,57].

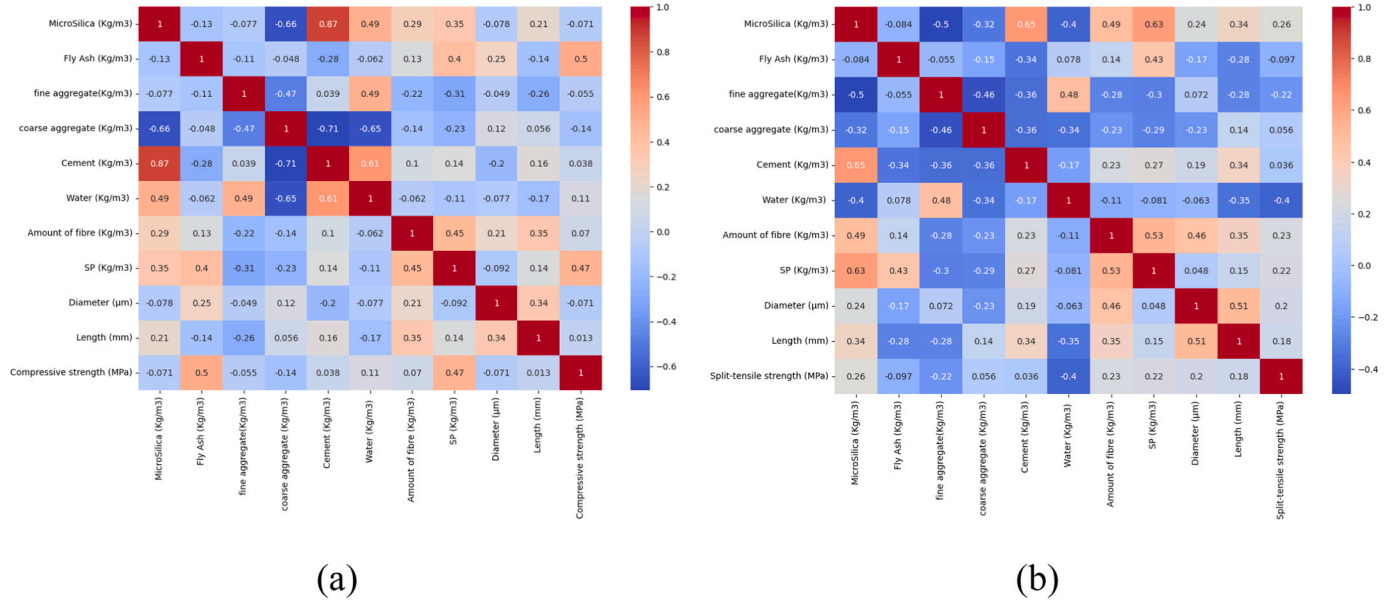

Fig. 4. Correlation matrix for the input and output parameters; (a) Compressive strength; (b) Split tensile strength.

Key hyperparameters such as tree depth, minimum samples for splitting nodes, minimum samples at leaf nodes, and maximum input features per node are optimized to achieve the best model performance, which has been done in this study. Although decision trees are easy to interpret and visualize, a single tree may not capture the complexity of the data, leading to overfitting and challenges with variance and bias.

3.6.3. *Random forest regression*

Random Forest Regression (RFR) is an ensemble learning technique that enhances prediction accuracy by combining multiple decision trees. Each decision tree is trained on a random subset of the training data and a random subset of input features. The final prediction is obtained by averaging the predictions from all the trees. This method, known as bootstrap aggregation or bagging, involves creating random subsets (bootstrap samples) of the dataset to train each tree. The use of different bootstrap samples for each tree increases the model's robustness and reduces the risk of overfitting [58,59].

3.6.4. *Extra tree regressor*

Extra Trees Regression (ETR) builds on the Random Forest method to improve prediction accuracy by generating and combining many diverse decision trees. It achieves this by randomly selecting feature subsets and split points for each feature at each node, creating a more varied ensemble. The final prediction is the average of the predictions from all trees. ETR is particularly robust against noisy or irrelevant features, often leading to superior model performance [60].

3.6.5. *Gradient tree boosting regression*

Gradient Tree Boosting Regression (GTBR) is an advanced machine learning algorithm used for regression and classification. It builds an ensemble of decision trees sequentially, with each tree correcting the errors of the previous one. Using gradient descent optimization, it iteratively minimizes the residuals between observed and predicted values. This approach results in a robust and accurate model, making GTBR a popular choice for various predictive modeling tasks [61].

3.6.6. *Extreme gradient boosting (XGBoost)*

XGBoost is a sequential boosting algorithm that combines multiple decision trees to create a robust model. Starting with an initial tree, it calculates the residuals between actual and predicted values. Each subsequent tree is designed to correct these residuals, refining the model layer by layer. This iterative process enhances the model's predictive accuracy by continuously adjusting to previous errors [62].

3.7. *Shapley Additive exPlanations (SHAP)*

Shapley Additive exPlanations (SHAP) is a method used to explain the impact of individual features on model predictions. Based on cooperative game theory, SHAP assigns each feature an importance value, ensuring a fair contribution distribution. This method enhances the interpretability of model outcomes by providing a detailed understanding of feature impacts. In this research, SHAP analysis will be applied to the best-performing model to examine feature contributions. Additionally, feature dependency plots will be analyzed to explore interactions between factors and their most dependent variables [63].

3.8. *User friendly interface*

A user-friendly interface was created using Gradio V4.36.1, a Python library for rapid interface generation, and deployed online via Hugging Face. After evaluating various machine learning models, the best-performing one will be selected for its superior predictive capabilities. This optimal model will be used to predict the compressive strength and split tensile strength of glass fibre concrete, ensuring precision and ease of use through the Gradio interface. The trained model file and source code are available at this link (https://huggingface.co/spaces/MohamedRabie26/Glass_fibre_concrete/tree/main).

4. Criteria for performance evaluation and hyperparameter selection

4.1. *Performance evaluation criteria*

Achieving optimal outcomes in statistical and data-driven models requires continuous performance assessment during training. In this study, each model's hyperparameters were optimized using the Optuna library, which performs efficient hyperparameter optimization. The ML models underwent 5-fold cross-validation on the training dataset, dividing it into five parts. In each iteration, four parts were used for training, and one part for performance assessment. The model with the best-performing hyperparameters was selected for predictions.

The performance of different ML models was evaluated using four

metrics: Mean Absolute Percentage Error (MAPE), Mean Absolute Error (MAE), Root Mean Squared Error (RMSE), and the Coefficient of Determination (R^2), as defined in Eqs. 1 to 4:

$$MAPE = \frac{100}{n}\sum_{i=1}^{n}\left|\frac{y_i - \hat{y}_i}{y_i}\right| \quad (1)$$

$$MAE = \frac{1}{n}\sum_{i=1}^{n}|y_i - \hat{y}_i| \quad (2)$$

$$RMSE = \sqrt{\frac{1}{n}\sum_{i=1}^{n}(y_i - \hat{y}_i)^2} \quad (3)$$

$$R^2 = 1 - \frac{\sum_{i=1}^{n}(y_i - \hat{y}_i)^2}{\sum_{i=1}^{n}(y_i - \bar{y})^2} \quad (4)$$

where y_i and $\hat{y}_i$ are the target and predicted values, respectively, $\bar{y}$ is the mean of values, and n is the number of data points.

A superior model exhibits lower MAE and RMSE values, coupled with a higher R^2 value. Where overfitting of a model shows higher error metrics on the test set compared to the training set and a significant discrepancy between training and test R^2 values.

4.2. Hyper parameter selection

Hyperparameters are crucial elements in defining the characteristics and learning process of a machine learning model, necessitating careful optimization for effective performance and accuracy. This study uses Optuna, a next-generation hyperparameter optimization framework known for its robustness and unique features, to optimize model hyperparameters. Compared to the traditional grid search method, Optuna is more efficient and flexible. Leveraging techniques from deep learning, Optuna efficiently handles high-dimensional and non-convex parameter spaces, a common challenge in ML model optimization. Its pruning feature stops unpromising trials early, saving computational resources and accelerating the optimization process. Further details on Optuna can be found in [64].

Table 4 presents a detailed overview of the optimized hyperparameter values and the best-performing settings, offering a comprehensive summary of the parameters that led to the model's optimal performance.

Table 4
Optuna optimized hyperparameters.

Model	hyperparameter Range	CS Value	ST Value
Support vector regression (SVR)	C: [0.1, 2000]	39.94	91.76
-	epsilon: [0.0001, 1]	0.00084	0.00057
-	gamma: [auto, scale]	auto	auto
-	kernel: [rbf, linear, poly, sigmoid]	rbf	poly
Decision tree (DT)	max_depth: [1500]	141	92
-	max_features: [1,50]	39	9
-	min_samples_leaf: [1,50]	1	1
-	min_samples_split: [0,1]	0.11	0.0990
-	random_state: [5]	5	5
Random forest regression (RFR)	max_depth: [10,50]	37	11
-	max_features: ['log2', 'sqrt']	log2	log2
-	min_samples_leaf: [1,40]	1	1
-	min_samples_split: [2,10]	2	2
-	n_estimators: [50,1000]	376	641
-	random_state: [5]	5	5
Extra tree regressor (ETR)	max_depth: [3,50]	14	37
-	max_features: ['log2', 'sqrt']	sqrt	sqrt
-	min_samples_leaf: [1,40]	1	1
-	min_samples_split: [2,10]	2	3
-	n_estimators: [10,1000]	734	590
-	random_state: [5]	5	5
Gradient tree boosting (GTB)	n_estimators: [50,1000]	867	463
-	max_depth: [4,8]	6	4
-	learning_rate: [0.02, 0.5]	0.0853	0.0905
-	subsample: [0.2, 0.5]	0.3354	0.3096
-	max_features: [7,50]	13	37
-	min_samples_split: [2,6]	6	2
-	min_samples_leaf: [1,40]	1	1
-	random_state: [5]	5	5
Extreme gradient boosting (XGBoosting)	n_estimators': [50,550],	500	393
-	'max_depth': [4,40],	4	18
-	'learning_rate': [0.05, 0.3],	0.1180	0.0881
-	'subsample': [0.2, 0.5],	0.2958	0.2680
-	'colsample_bylevel': [0.6, 0.7],	0.6505	0.6115
-	'colsample_bynode': [0.9, 1.0],	0.9526	0.9884
-	'colsample_bytree': [0.9, 1.0],	0.9895	0.9874
-	'reg_alpha': [0, 0.1],	0.000279	0.0097
-	'reg_lambda': [0.9, 1],	0.9475	0.9172
-	'gamma': [0.0, 0.1],	4.533e−05	3.972e−05
-	'random_state': [5]	5	5

5. Results and discussion

5.1. Experimental work

5.1.1. Fresh properties

The results of the slump test for GFC concrete, as illustrated in Fig. 5. The workability of different concrete mixes, including a control mix and three glass fibre concrete (GFC) mixes with varying fibre contents (G-1, G-2, and G-3). The control mix exhibited a slump value of 60 mm, establishing the baseline for comparison. The GFC mixes, identified as G-1 (0.12 % V_f), G-2 (0.22 % V_f), and G-3 (0.43 % V_f), all demonstrated a consistent slump value of 65 mm. This uniform increase in slump across the fibre-reinforced mixes, compared to the control mix, indicates that the inclusion of glass fibres within the tested volume fractions slightly enhances the workability of the concrete, which was consistent to the findings in the literature [65]. The consistent slump values among the GFC mixes suggest that the addition of fibres, up to 0.43 %, does not significantly hinder the workability, thereby ensuring proper compaction and consolidation during placement.

5.1.2. Hardened properties

The compressive strength results indicate that the inclusion of glass fibres impacts concrete performance at both 7 and 28 days as shown in Fig. 6. The control mix had compressive strengths of 20.807 MPa at 7 days and 29.973 MPa at 28 days. The G-1 mix, with 0.12 % fibres, recorded 18.477 MPa at 7 days (an 11 % reduction) and 29.613 MPa at 28 days (a 1 % reduction), suggesting minimal long-term impact. Conversely, the G-2 mix with 0.22 % fibres showed significant reductions, with 16.167 MPa at 7 days (22 % decrease) and 25.390 MPa at 28 days (15 % decrease). The G-3 mix, containing 0.43 % fibres, had 18.467 MPa at 7 days (11 % decrease) and 26.327 MPa at 28 days (12 % decrease). These results highlight that higher fibre contents consistently impair compressive strength, whereas a moderate fibre content (G-1) shows potential for minimal adverse effects over time.

The split tensile strength results demonstrate the varying effects of glass fibre content on concrete as illustrated in Fig. 7. The control mix exhibited a split tensile strength of 2.004 MPa. The G-1 mix, with 0.12 % fibres, showed a slight increase to 2.017 MPa, reflecting a 1 % improvement. The G-2 mix, containing 0.22 % fibres, significantly enhanced the split tensile strength to 3.415 MPa, marking a substantial 70 % increase. Similarly, the G-3 mix with 0.43 % fibres achieved a split

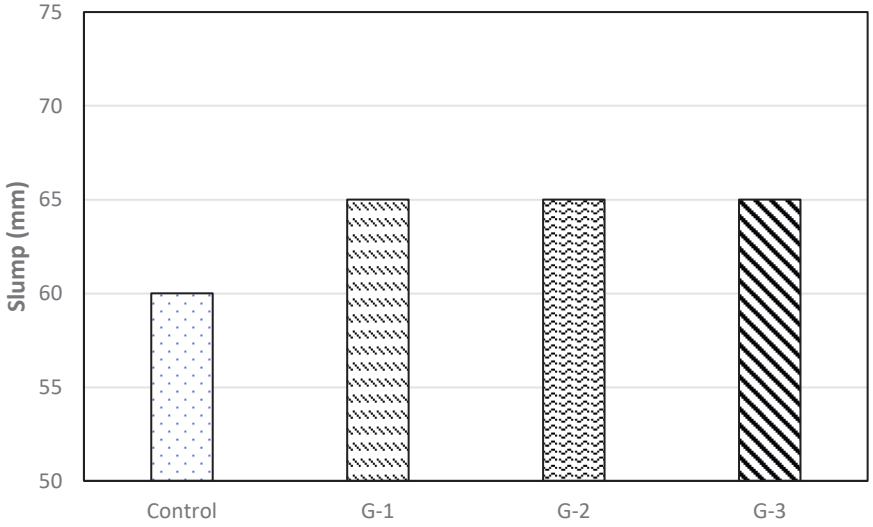

Fig. 5. Slump test results.

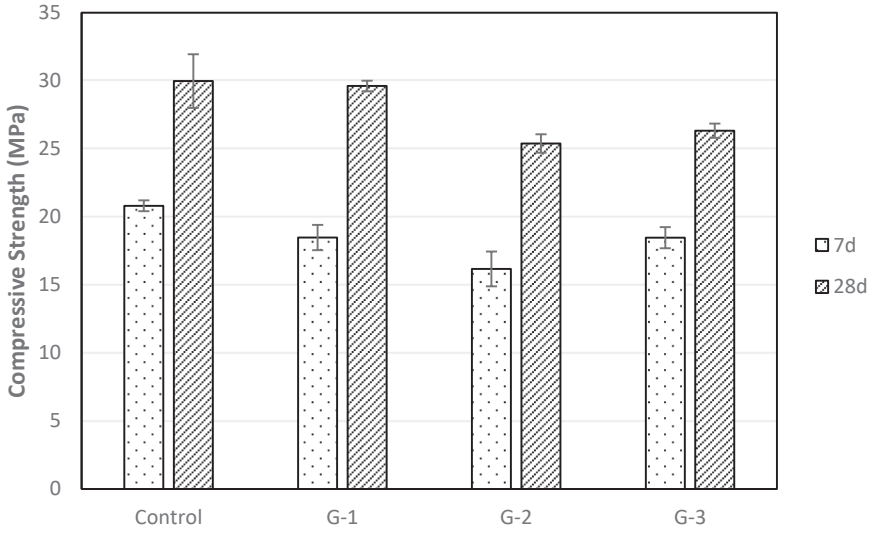

Fig. 6. Compressive strength results for 7 days and 28 days.

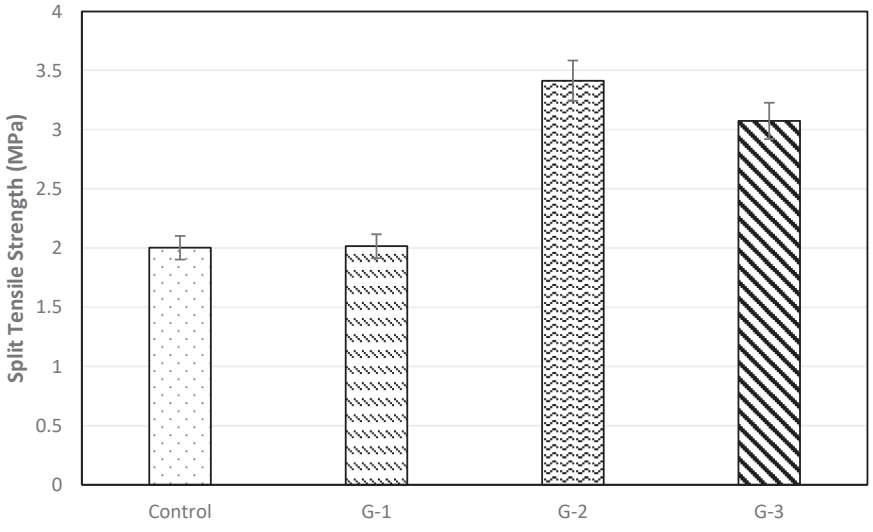

Fig. 7. Split tensile strength of glass fibre concrete.

tensile strength of 3.075 MPa, corresponding to a 53 % increase. These results indicate that increasing glass fibre content positively influences the split tensile strength, with the most notable improvement observed at 0.22 % fibre content.

The observed differences in compressive and split tensile strength results for glass fibre concrete (GFC) are due to several factors. In compressive strength tests, higher fibre content can introduce micro-cracks and weak points, leading to reduced strength, while in split tensile strength tests, fibres effectively bridge cracks, enhancing tensile capacity [66]. The orientation and distribution of fibres, along with the fibre-matrix bonding, play crucial roles; fibres tend to align and bond better under tensile stress, improving tensile strength significantly [67, 68]. Additionally, higher fibre content can cause stress concentrations and non-uniform stress distribution in compressive loading, further reducing compressive strength. These factors collectively explain why higher fibre content improves split tensile strength but impairs compressive strength.

5.1.3. Rate of water absorption

The results for the rate of water absorption are shown in Fig. 8. The control mix shows a gradual increase in capillary absorption from 0.000422 g/mm^2 at 1 minute to 0.006936 g/mm^2 at 10,080 minutes.

In contrast, the GFC mixes exhibit higher initial and long-term absorption rates. At 1 minute, G-1, G-2, and G-3 have absorption rates of 0.00084 g/mm^2, 0.00064 g/mm^2, and 0.0006933 g/mm^2, respectively. Over time, these rates increase more significantly compared to the control. At 10,080 minutes, G-1 reaches 0.01 g/mm^2, G-2 reaches 0.01001 g/mm^2, and G-3 reaches 0.0103911 g/mm^2.

The increased absorption rates in the GFC mixes suggest that the inclusion of glass fibres, particularly at higher percentages, leads to greater porosity and micro-cracking, facilitating more water ingress [13]. G-3, with the highest fibre content (0.43 % V_f), consistently shows the highest absorption values across all time points, indicating the most significant increase in permeability. These findings highlight the necessity to balance the mechanical benefits of fibre reinforcement with potential impacts on concrete durability, especially regarding water absorption and long-term performance.

5.1.4. Bulk density

Fig. 9 illustrates the bulk density (kg/m^3) of the control mix and three glass fibre reinforced concrete (GFC) mixes with varying fibre contents (G-1, G-2, and G-3). The control mix shows the highest bulk density at approximately 2195 kg/m^3 . The G-1 mix (0.12 % V_f) has a slightly lower bulk density, around 2185 kg/m^3 . The bulk density further decreases with increasing fibre content, with the G-2 mix (0.22 % V_f) at approximately 2170 kg/m^3 and the G-3 mix (0.43 % V_f) at around 2150 kg/m^3 . This trend suggests that the inclusion of glass fibres reduces the overall density of the concrete, likely due to the lightweight nature of the fibres and the increased void content resulting from fibre dispersion.

5.1.5. Moisture content

Fig. 10 displays the moisture content (%) of the control mix and the three GFC mixes. The control mix has a moisture content of about 5 %. The G-1 mix shows a slight increase to approximately 5.2 %. The G-2 and G-3 mixes exhibit further increases in moisture content, with values around 5.8 % and 6.2 %, respectively. These results indicate that the addition of glass fibres, particularly at higher contents, increases the moisture content of the concrete. This could be attributed to the higher porosity and larger surface area introduced by the fibres, which enhances the concrete's ability to absorb and retain moisture [13].

5.2. Performance of ML models

5.2.1. Compressive strength

Table 5 presents the performance indices for compressive strength prediction using various machine learning (ML) models, evaluated across training, test, and whole datasets as shown in Fig. 11. The metrics considered are Mean Absolute Percentage Error (MAPE), Mean Absolute Error (MAE), Root Mean Squared Error (RMSE), and the Coefficient of Determination (R^2).

SVR demonstrated a MAPE of 9.07 % on the training dataset and 6.77 % on the test dataset. The MAE and RMSE for the training dataset were 0.053 MPa and 0.110 MPa, respectively, with an R^2 of 0.784. For the test dataset, the MAE was 0.060 MPa, the RMSE was 0.084 MPa, and the $R^2$was 0.837. These results indicate moderate accuracy, with better performance on the test dataset compared to training.

The Decision Tree model achieved a MAPE of 6.71 % on the training dataset and 7.88 % on the test dataset. The training dataset showed an MAE of 0.052 MPa and an RMSE of 0.071 MPa, with an $R^2$of 0.912. The test dataset results included an MAE of 0.066 MPa, an RMSE of 0.108 MPa, and an $R^2$of 0.734. The DT model exhibited strong performance on the training data but showed a decrease in accuracy on the test data.

RFR displayed a MAPE of 3.11 % on the training dataset and 4.88 % on the test dataset. The training dataset had an MAE of 0.021 MPa and an RMSE of 0.030 MPa, with an $R^2$of 0.986. On the test dataset, the MAE was 0.039 MPa, the RMSE was 0.049 MPa, and the R^2 was 0.946. These results highlight RFR's high accuracy and robustness, particularly on the training dataset.

ETR yielded a MAPE of 9.07 % on the training dataset and 3.90 % on the test dataset. The MAE and RMSE for the training dataset were

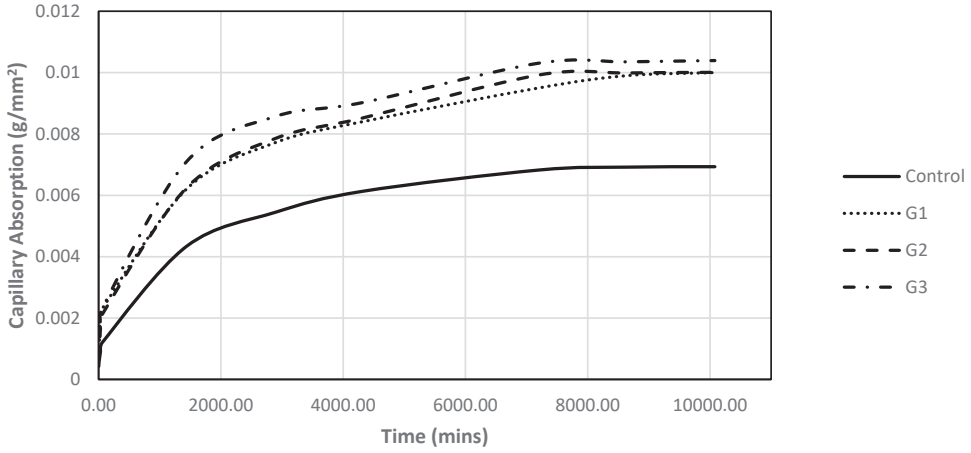

Fig. 8. Rate of Water absorption for control and glass fibre concrete.

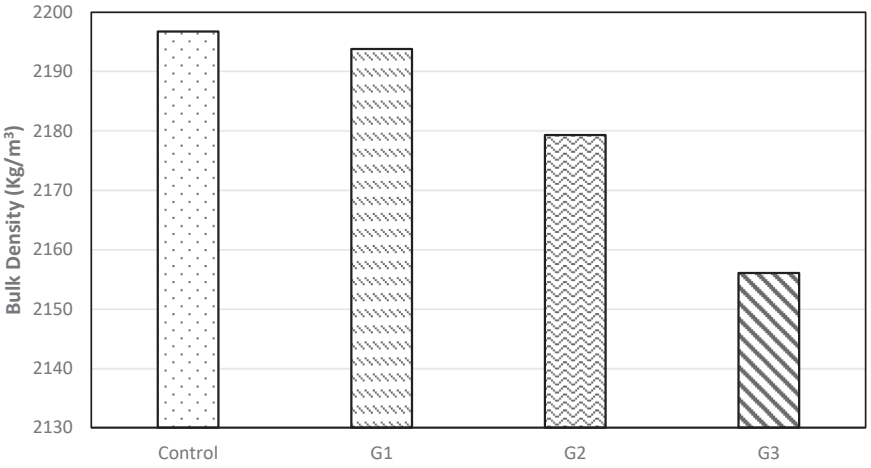

Fig. 9. Bulk density of control and glass fibre concrete.

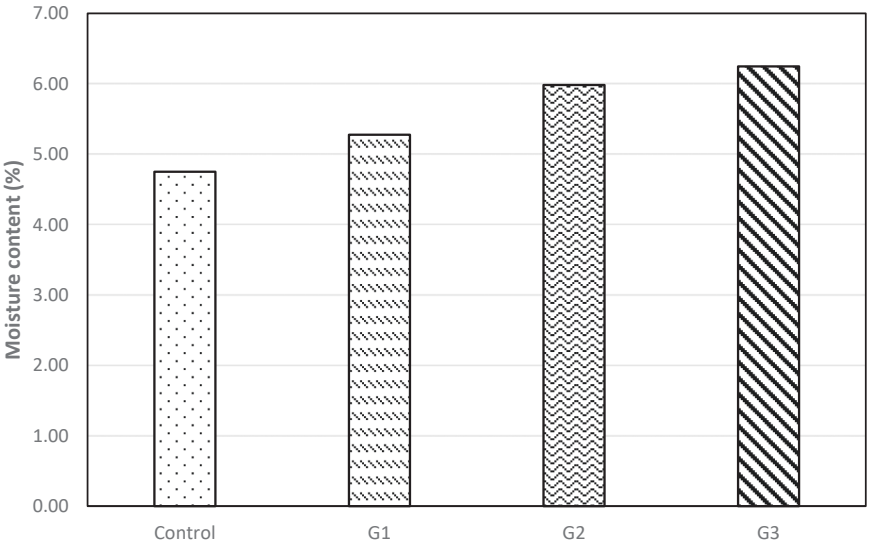

Fig. 10. Moisture content for control and glass fibre concrete.

Table 5
Performance indices for different ML algorithms in predicting the compressive strength of GFC.

	Training dataset				Test dataset			
Models	MAPE (%)	MAE (MPa)	RMSE (MPa)	R^2	MAPE (%)	MAE (MPa)	RMSE (MPa)	R^2
SVR	9.07	0.053	0.110	0.784	6.77	0.060	0.084	0.837
DT	6.71	0.052	0.071	0.912	7.88	0.066	0.108	0.734
RFR	3.11	0.021	0.030	0.986	4.88	0.039	0.049	0.946
ETR	9.07	0.053	0.110	0.784	3.90	0.031	0.045	0.954
GTBR	0.00	1.31E−08	2.13E−08	1.000	3.53	0.030	0.037	0.968
XGBoosting	0.70	0.0051	0.007	0.999	4.20	0.035	0.048	0.948

0.053 MPa and 0.110 MPa, respectively, with an $R^2$of 0.784. For the test dataset, the MAE was 0.031 MPa, the RMSE was 0.045 MPa, and the $R^2$was 0.954. This model showed excellent performance on the test dataset, indicating strong generalization ability.

GTBR achieved exceptional results with a MAPE of 0.00 % on the training dataset and 3.53 % on the test dataset. The MAE and RMSE for the training dataset were negligible, with an $R^2$of 1.000. For the test dataset, the MAE was 0.030 MPa, the RMSE was 0.037 MPa, and the $R^2$was 0.968. These metrics demonstrate GTBR's superior performance, particularly in terms of accuracy and predictive reliability.

XGBoosting also performed excellently, with a MAPE of 0.70 % on the training dataset and 4.20 % on the test dataset. The MAE and RMSE for the training dataset were 0.0051 MPa and 0.007 MPa, respectively, with an $R^2$of 0.999. On the test dataset, the MAE was 0.035 MPa, the RMSE was 0.048 MPa, and the $R^2$was 0.948. These results indicate that XGBoosting is highly accurate and reliable across datasets.

Among the models evaluated, the Gradient Tree Boosting Regression (GTBR) emerged as the best performer, exhibiting near-perfect accuracy on the training dataset and maintaining high performance on the test dataset. This model's superior metrics, including the lowest MAPE and high R^2 values across datasets, underscore its robustness and reliability for predicting compressive strength.

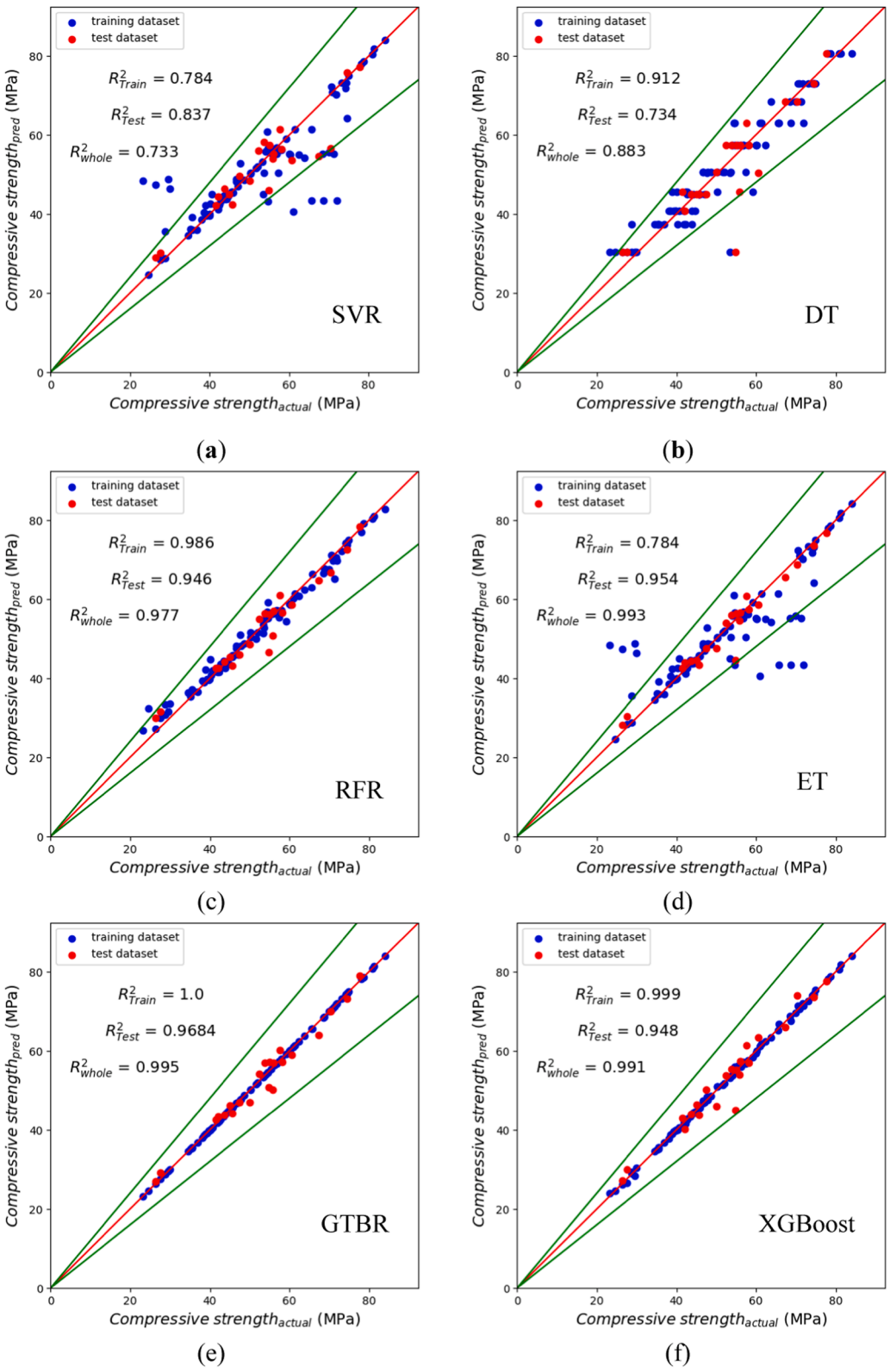

Fig. 11. Comparison of experimental and predicted compressive strength based on different ML algorithms; (a) SVR; (b) DT; (c) random forest; (d) extremely randomized trees; (e) gradient tree boosting; and (f) XGBoost.

5.2.2. Split tensile strength

Table 6 presents performance indices for predicting split tensile strength using various machine learning (ML) models, evaluated across training, test, and whole datasets as shown in Fig. 12.

The SVR model achieved a MAPE of 5.50 % on the training dataset and 14.60 % on the test dataset. The MAE and RMSE for the training dataset were 0.018 MPa and 0.034 MPa, respectively, with an $R^2$of 0.949. For the test dataset, the MAE was 0.066 MPa, the RMSE was 0.109 MPa, and the R^2 was 0.767. These results indicate good training performance but significantly lower accuracy on the test dataset, sug-

Table 6
Performance indices for different ML algorithms in predicting the split tensile strength of GFC.

	Training dataset				Test dataset			
Models	MAPE (%)	MAE (MPa)	RMSE (MPa)	R^2	MAPE (%)	MAE (MPa)	RMSE (MPa)	R^2
SVR	5.50	0.018	0.034	0.949	14.60	0.066	0.109	0.767
DT	5.20	0.025	0.034	0.957	10.32	0.054	0.09	0.843
RFR	2.61	0.010	0.016	0.989	10.96	0.052	0.085	0.859
ETR	5.50	0.018	0.034	0.949	12.07	0.054	0.089	0.846
GTBR	0.00	1.20E−06	1.59E−06	1.000	6.40	0.033	0.048	0.954
XGBoosting	1.78	0.008	0.010	0.996	9.78	0.046	0.071	0.900

gesting potential overfitting.

The Decision Tree model showed a MAPE of 5.20 % on the training dataset and 10.32 % on the test dataset. The MAE and RMSE for the training dataset were 0.025 MPa and 0.034 MPa, respectively, with an $R^2$of 0.957. On the test dataset, the MAE was 0.054 MPa, the RMSE was 0.090 MPa, and the R^2 was 0.843. The DT model demonstrated strong training performance and reasonable accuracy on the test dataset, indicating balanced performance.

The RFR model exhibited a MAPE of 2.61 % on the training dataset and 10.96 % on the test dataset. The MAE and RMSE for the training dataset were 0.010 MPa and 0.016 MPa, respectively, with an R^2 of 0.989. For the test dataset, the MAE was 0.052 MPa, the RMSE was 0.085 MPa, and the R^2 was 0.859. These results highlight RFR's high accuracy on the training data and robust performance on the test data.

The ETR model achieved a MAPE of 5.50 % on the training dataset and 12.07 % on the test dataset. The MAE and RMSE for the training dataset were 0.018 MPa and 0.034 MPa, respectively, with an R^2 of 0.949. For the test dataset, the MAE was 0.054 MPa, the RMSE was 0.089 MPa, and the R^2 was 0.846. This model demonstrated balanced performance across both datasets, with slightly better generalization than SVR.

The GTBR model excelled with a MAPE of 0.00 % on the training dataset and 6.40 % on the test dataset. The MAE and RMSE for the training dataset were negligible, with an R^2 of 1.000. On the test dataset, the MAE was 0.033 MPa, the RMSE was 0.048 MPa, and the R^2 was 0.954. These metrics illustrate GTBR's superior accuracy and predictive reliability, particularly on the test data.

XGBoosting also performed exceptionally well, with a MAPE of 1.78 % on the training dataset and 9.78 % on the test dataset. The MAE and RMSE for the training dataset were 0.008 MPa and 0.010 MPa, respectively, with an R^2 of 0.996. For the test dataset, the MAE was 0.046 MPa, the RMSE was 0.071 MPa, and the R^2 was 0.900. These results indicate XGBoosting's high accuracy and reliability across datasets.

Among the models evaluated, the Gradient Tree Boosting Regression (GTBR) emerged as the best performer, showing near-perfect accuracy on the training dataset and maintaining excellent performance on the test dataset. Its superior metrics, including the lowest MAPE and highest R^2 values, underscore its robustness and reliability for predicting split tensile strength.

5.3. Explainability and feature importance

The SHAP analysis reveals distinct patterns in how various features influence compressive strength and split tensile strength of concrete. As shown in Fig. 13 for compressive strength, fly ash emerges as the most critical factor, negatively impacting strength as its content increases. Cement content, however, plays a vital role in enhancing compressive strength, consistent with its function as a primary binding agent in concrete. Fine aggregate and water content also significantly influence compressive strength, with higher water content leading to reduced strength due to increased porosity.

In contrast as shown in Fig. 14, for split tensile strength, fine aggregate is the most influential feature, positively affecting the tensile capacity of concrete. Cement content again shows a strong positive impact, indicating its fundamental role in both compressive and tensile properties. Interestingly, the amount of fibre has a more pronounced positive effect on split tensile strength than on compressive strength, highlighting the fibres' role in improving concrete's resistance to tensile stresses. Fibers enhance the split tensile strength by bridging cracks and providing additional tensile capacity within the concrete matrix. This enhancement underscores the importance of fibre content in applications where tensile strength is critical, such as in pavements and precast concrete elements.

Water content's negative impact on tensile strength aligns with its effect on compressive strength, further emphasizing the importance of optimal water-cement ratios in concrete mix designs. The presence of superplasticizers (SP) and other admixtures also plays a role, though to a lesser extent, in fine-tuning the properties of both types of strength.

Overall, the SHAP analysis underscores the need to tailor concrete mix designs to balance both compressive and tensile properties, considering the distinct influences of various features. These insights are crucial for developing high-performance concrete with optimized mechanical properties for diverse structural applications.

5.4. User-friendly interface

user-friendly interface has been developed and deployed online, accessible through the following link: (https://huggingface.co/spaces/MohamedRabie26/Glass_fibre_concrete). This tool allows users to utilize the optimum machine learning model identified in this study, the Gradient Tree Boosting Regression (GTBR) model, to predict the compressive and split tensile strengths of glass fibre concrete. The tool leverages the ten factors investigated in this study for its predictions.

The interface features sliders that enable users to select values within the range of the data collected, ensuring accurate predictions based on the trained ML models and dataset. To switch between models, users can click on the "Split Tensile Strength" tab in the top left corner for split tensile strength predictions and click the corresponding tab for compressive strength predictions. Fig. 15 provides a screenshot of the tool, illustrating its application for both compressive and split tensile strength predictions of glass fibre concrete. This tool facilitates easy and precise assessments, making it an invaluable resource for practitioners and researchers in the field.

6. Conclusions

In this research, extensive experimental work was conducted to evaluate the mechanical and durability properties GFC focusing on compressive strength and split tensile strength, which are crucial in civil engineering. The experimental data was combined with a dataset sourced from previous studies, encompassing 108 data points for compressive strength and 87 for split tensile strength. Various machine learning (ML) algorithms were examined, including Support Vector Regression (SVR), Decision Tree (DT), Random Forest Regression (RFR), Extra Trees Regressor (ETR), Gradient Tree Boosting (GTBR), and Extreme Gradient Boosting (XGBoosting). The dataset was split, with 80 % allocated for training and 20 % for testing. Optuna library was

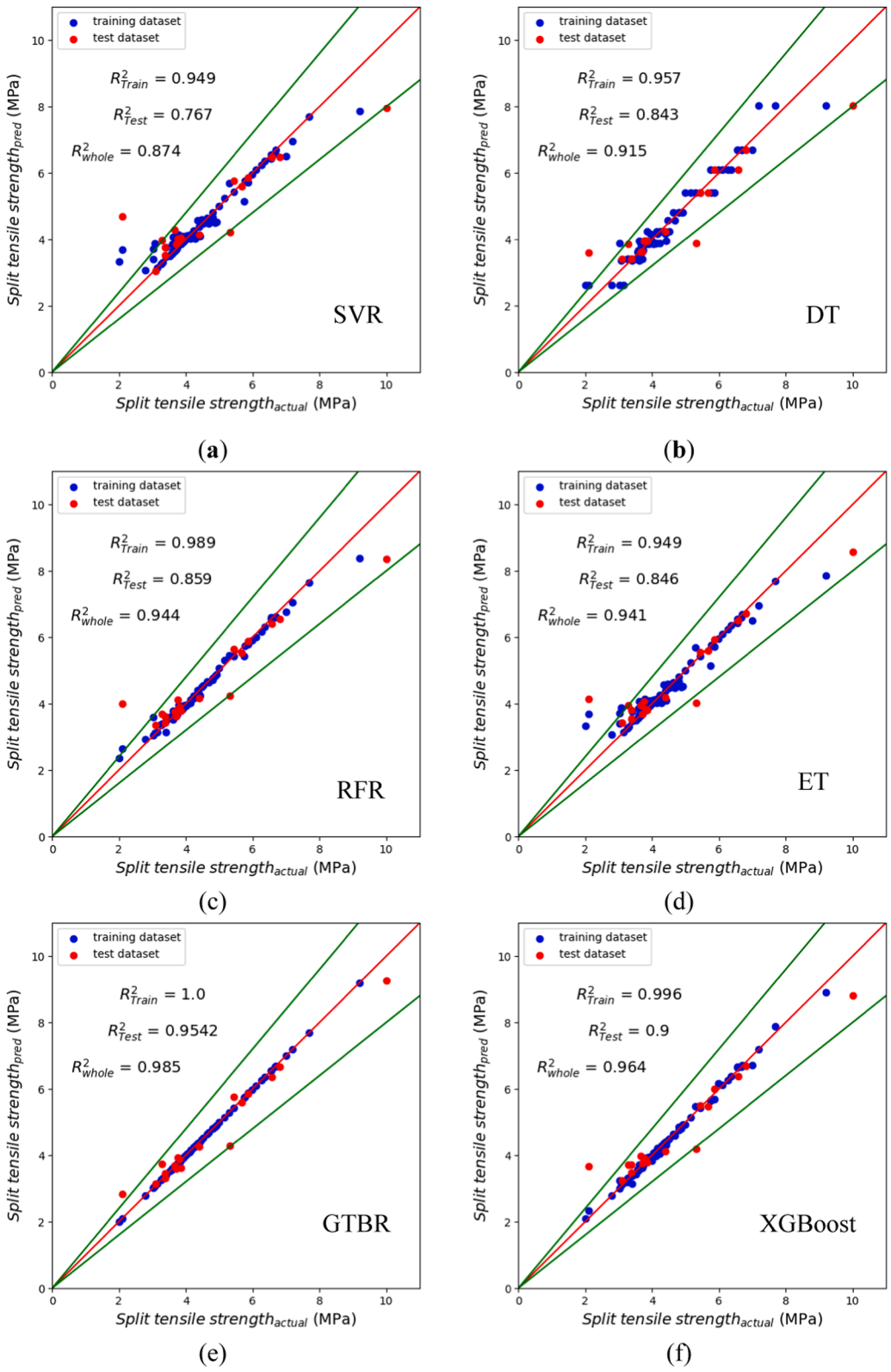

Fig. 12. Comparison of experimental and predicted split tensile strength based on different ML algorithms; (a) SVR; (b) DT; (c) random forest; (d) extremely randomized trees; (e) gradient tree boosting; and (f) XGBoost.

used for hyperparameter optimization. Model performance was assessed using key statistical indicators such as MAE, MAPE, RMSE, and R^2. Additionally, SHAP (Shapley Additive exPlanations) analysis was employed to determine the influence of each feature on the models' predictions, providing deeper insights into feature importance. This approach integrates rigorous experimental work with advanced ML techniques to enhance the predictability of GFC properties.

From the presented study, the following key conclusions can be drawn:

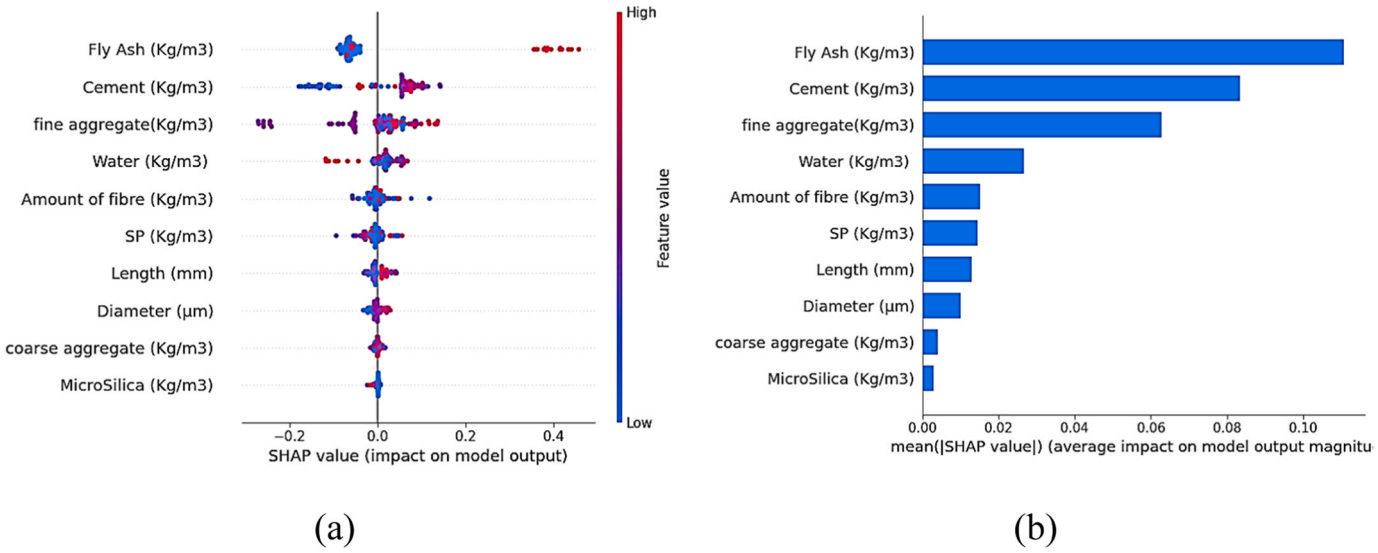

Fig. 13. SHAP analysis; (a) SHAP summary plot of the compressive strength predictions (MPa); (b) ranking of feature's impact on the prediction model.

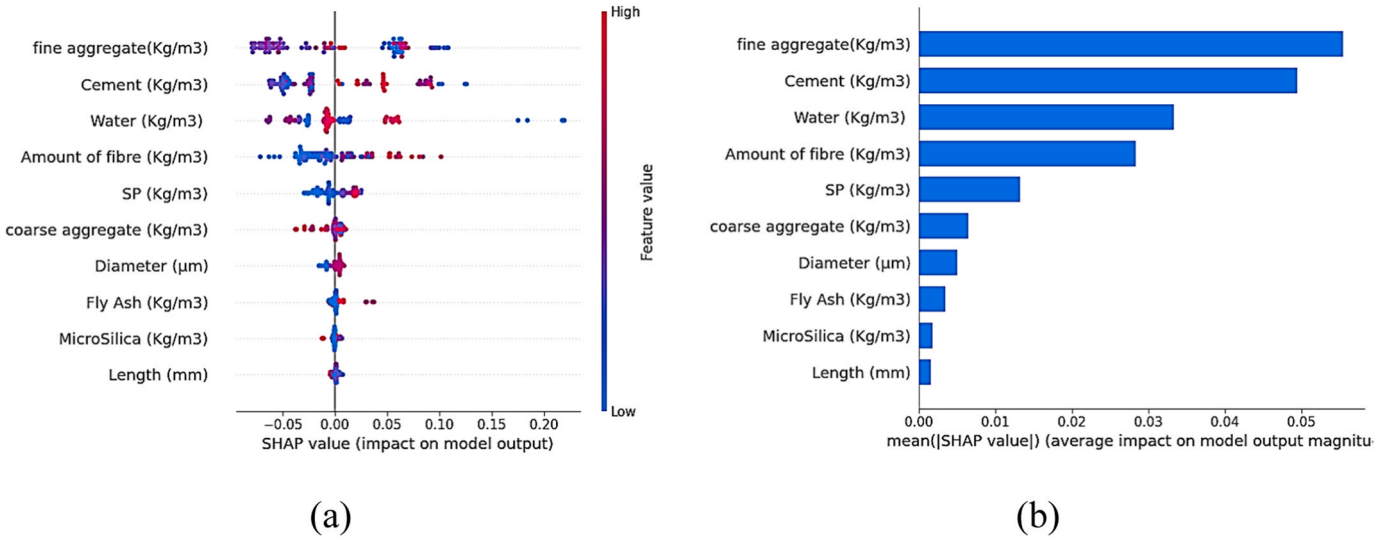

Fig. 14. SHAP analysis; (a) SHAP summary plot of the split tensile strength predictions (MPa); (b) ranking of feature's impact on the prediction model.

- The inclusion of glass fibres in concrete showed varying effects on compressive and split tensile strengths.
- The G-1 mix (0.12 % fibres) had a minimal impact on compressive strength, with an 11 % reduction at 7 days and a 1 % reduction at 28 days.
- Higher fibre content (G-2 with 0.22 % and G-3 with 0.43 %) resulted in more significant reductions in compressive strength, with decreases up to 22 % at 7 days and 15 % at 28 days.
- Split tensile strength was positively influenced by higher fibre content, with the G-2 mix showing a 70 % increase and the G-3 mix showing a 53 % increase compared to the control mix at 28 days.
- Gradient Tree Boosting (GTBR): Emerged as the most accurate model for both the compressive strength and split tensile strength of GFC.
- SHAP analysis indicated that factors such as fine aggregate content, cement content, and the amount of glass fibre significantly influenced the models' predictions, highlighting their critical roles in determining the mechanical properties of GFC.
- An online user-friendly interface was developed to enable academics and professionals to efficiently estimate the mechanical properties of GFC based on the optimum ML model. This tool, featuring interactive sliders for input variables, ensures precise predictions within the collected data range.

These findings demonstrate the effectiveness of integrating experimental work with advanced ML techniques to enhance the predictability and understanding of GFC properties, ultimately contributing to more efficient and durable concrete formulations.

CRediT authorship contribution statement

Shaaban Ibrahim G.: Writing – review & editing, Validation,

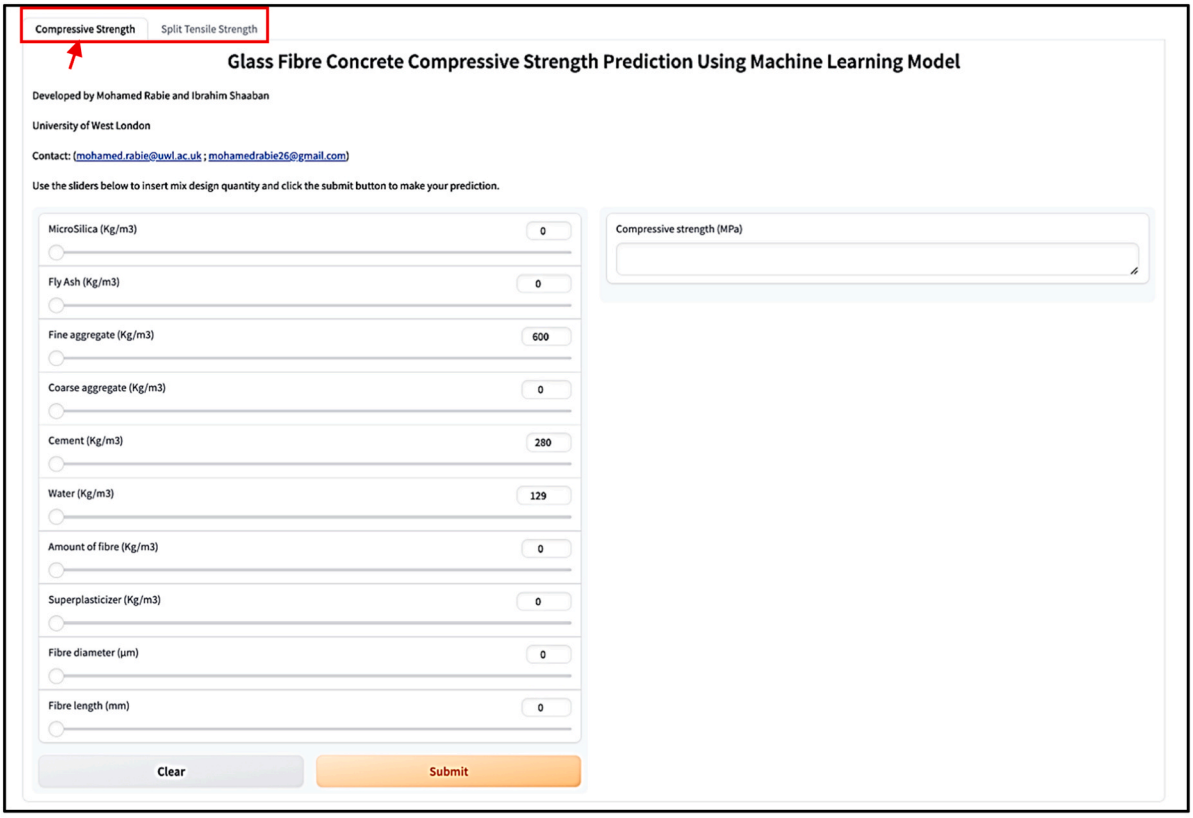

(a)

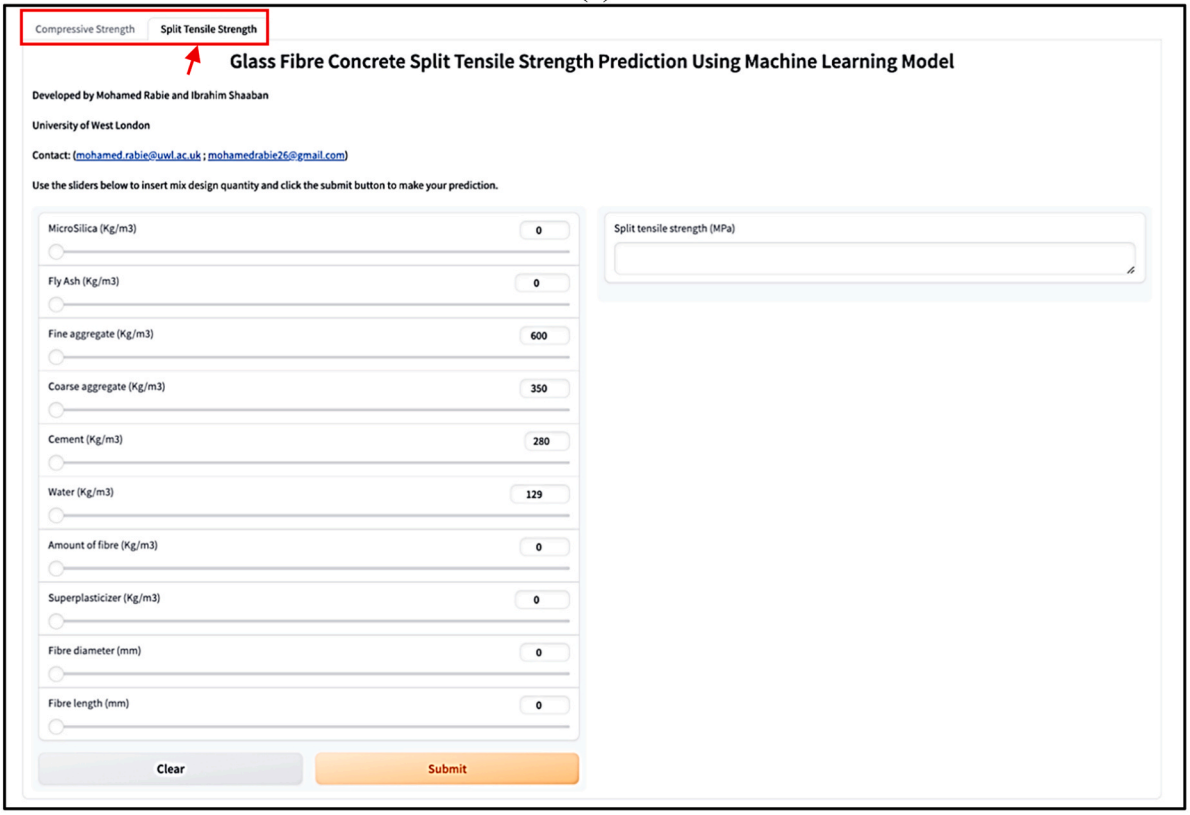

(b)

Fig. 15. Glass fibre concrete prediction tool; (a) Compressive strength prediction; (b) Split tensile strength prediction.

Supervision, Resources, Project administration, Funding acquisition, Conceptualization. **Rabie Mohamed:** Writing – review & editing, Writing – original draft, Visualization, Software, Methodology, Investigation, Formal analysis, Data curation, Conceptualization.

Declaration of Competing Interest

The authors declare that they have no known competing financial interests or personal relationships that could have appeared to influence the work reported in this paper.

Acknowledgement

This work was partially funded by the UWL Vice Chancellor's Scholarship awarded to the first author.

Appendix A

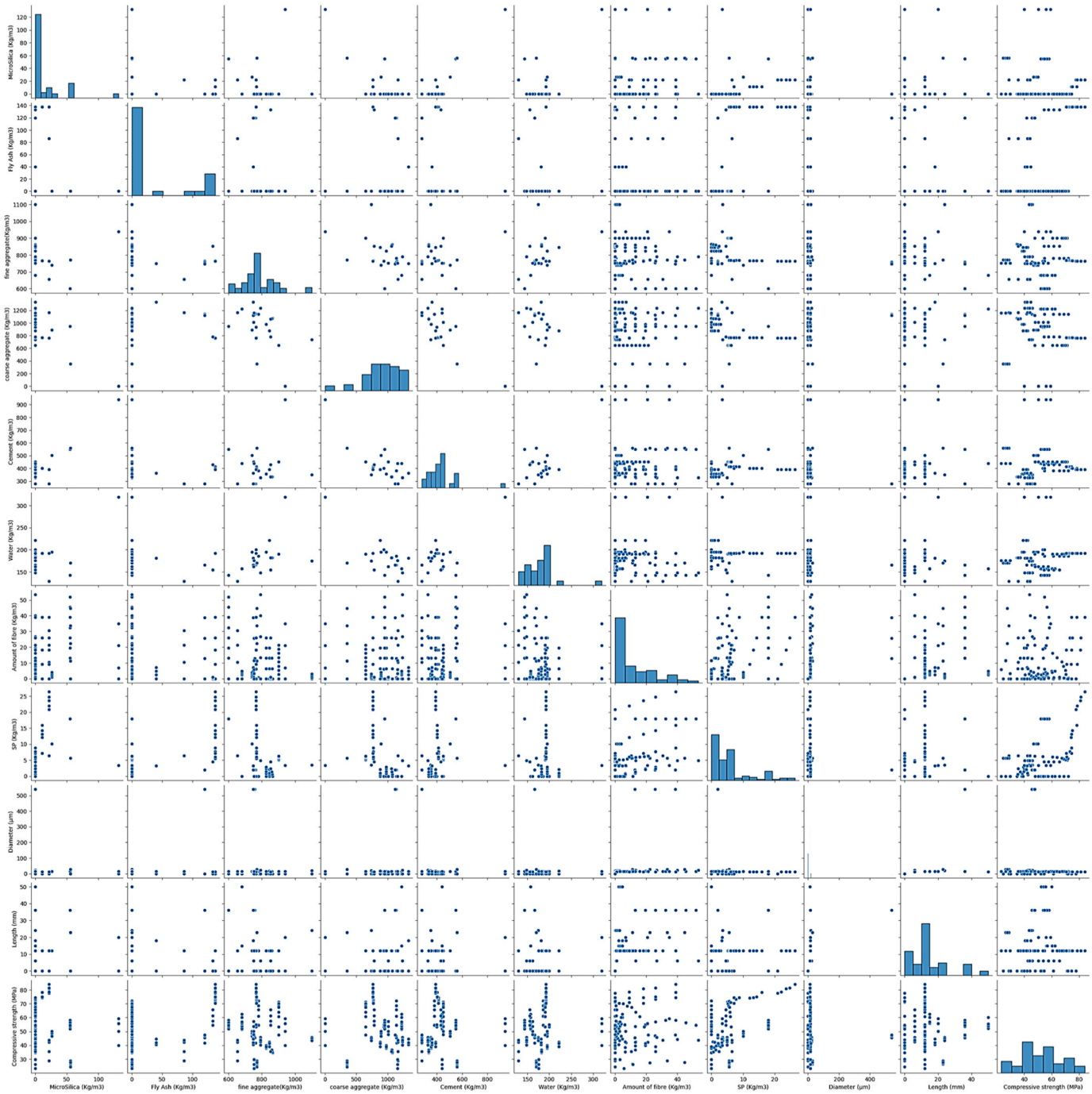

Figure A1. Pair plots for the dataset parameters for compressive strength of GFC

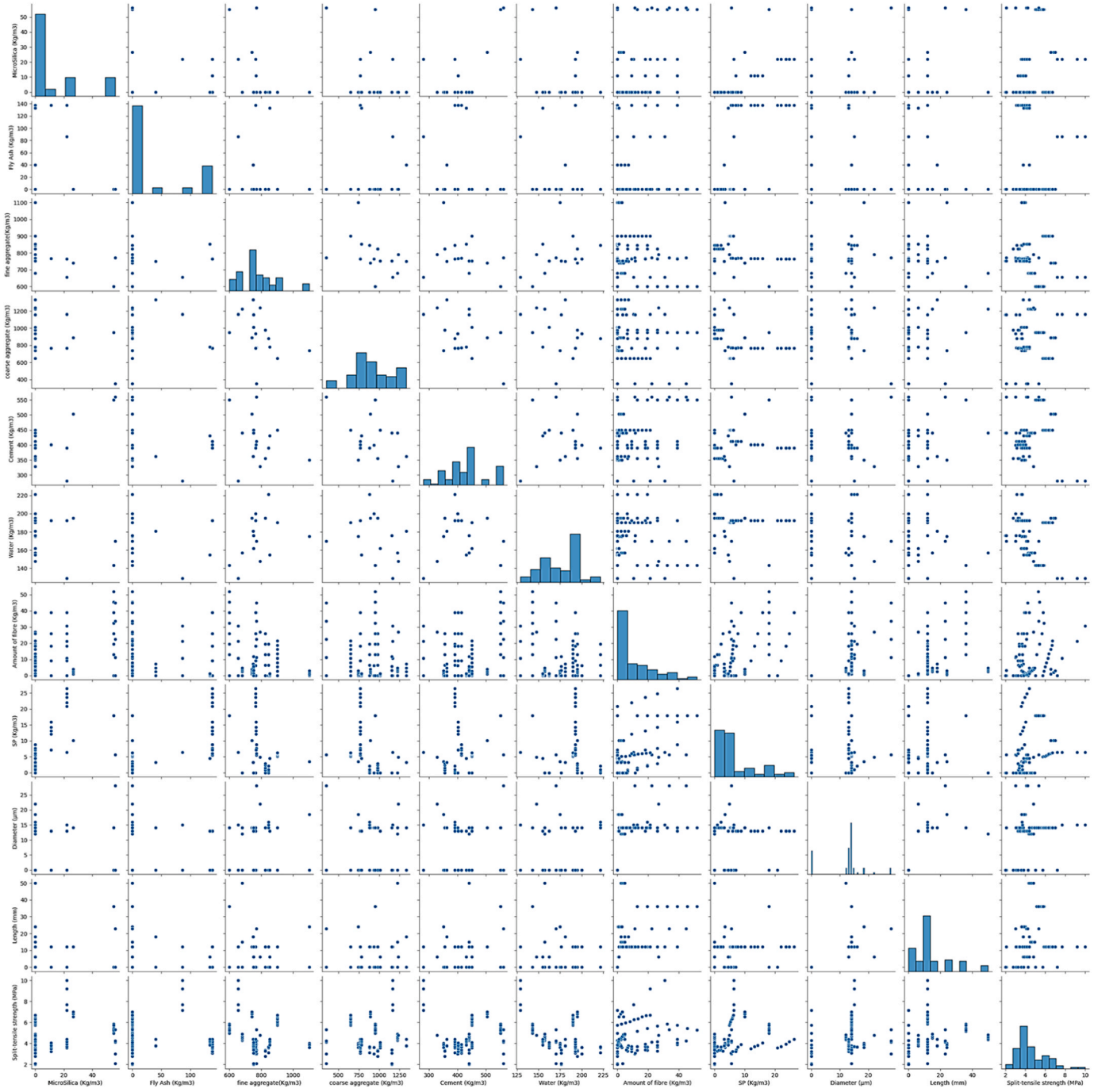

Figure A2. Pair plots for the dataset parameters for split tensile strength of GFC

Appendix B

Dataset parameters for compressive strength of GFC

MicroSilica (Kg/m^3)	Fly Ash (Kg/m^3)	Fine aggregate (Kg/m^3)	Coarse aggregate (Kg/m^3)	Cement (Kg/m^3)	Water (Kg/m^3)	Amount of fibre (Kg/m^3)	SP (Kg/m^3)	Diameter (μm)	Length (mm)	Compressive strength (MPa)
0	0	780	1140	380	186	0	0	0	0	61
0	0	780	1140	380	186	0.19	0	14	12	65.67
0	0	780	1140	380	186	0.38	0	14	12	72
0	0	780	1140	380	186	0.57	0	14	12	68.67
0	0	780	1140	380	186	0.76	0	14	12	54.67
0	0	680	1225	440	157	0	0	0	0	51.582
0	0	680	1225	440	157	2.4	0	12	50	52.34
0	0	680	1225	440	157	3.2	0	12	50	54.044
0	0	680	1225	440	157	4	0	12	50	55.432
0	0	680	1225	440	157	4.8	0	12	50	60
0	0	680	1225	440	157	2.4	0	14	15	56.014
0	0	680	1225	440	157	3.2	0	14	15	56.77
0	0	680	1225	440	157	4	0	14	15	60.26
0	0	680	1225	440	157	4.8	0	14	15	62.417
0	0	1100	740	350	175	0	3.5	0	0	43.916
0	0	1100	740	350	175	0.5	3.5	18.5	24	45.66
0	0	1100	740	350	175	1	3.5	18.5	24	45.916
0	0	1100	740	350	175	2	3.5	18.5	24	45
0	0	1100	740	350	175	3	3.5	18.5	24	43.416
0	0	765	935	400	200	0	0	0	0	53.38
0	0	765	935	400	200	6.25	0	14	12	54.77
26.5	0	740	890	503.5	195	1.007	10.07	14	12	46.75
26.5	0	740	890	503.5	195	2.014	10.07	14	12	48.7
26.5	0	740	890	503.5	195	3.021	10.07	14	12	50.05
26.5	0	740	890	503.5	195	4.028	10.07	14	12	46.72
0	120	764	1147	280	166	0	2	0	0	41.8
0	120	759	1138	280	166	12.9	2	540	36	45.6
0	120	754	1130	280	166	25.8	2	540	36	47
0	120	748	1122	280	166	38.7	2	540	36	47.5
0	0	825	980	355	195	0	0	0	0	38.027
0	0	825	980	355	195	6.5	0.89	14	12	38.583
0	0	825	980	355	195	13	1.45	14	12	39.76
0	0	825	980	355	195	19.5	2.31	14	12	39.88
0	0	825	980	355	195	26	2.84	14	12	39.22
22	86	655	1165	280	129	0	6.45	0	0	28.8
22	86	655	1165	280	129	10.62	6.45	15	12	35.5
22	86	655	1165	280	129	21.24	6.45	15	12	42.2
22	86	655	1165	280	129	30.68	6.45	15	12	43.9
55	0	600	950	550	143	0	18	0	0	52
55	0	600	950	550	143	13	18	14	36	53.75
55	0	600	950	550	143	19.5	18	14	36	55
55	0	600	950	550	143	26	18	14	36	56.84
55	0	600	950	550	143	32.5	18	14	36	58.12
55	0	600	950	550	143	39	18	14	36	58
55	0	600	950	550	143	45.5	18	14	36	56.3
55	0	600	950	550	143	52	18	14	36	54.67
0	0	791.27	1237.8	328.33	147.74	0	4.92	0	0	40.2
0	0	791.27	1237.8	328.33	147.74	13.4	4.92	22	6	42.6
0	0	791.27	1237.8	328.33	147.74	26.8	4.92	22	6	45.7
0	0	791.27	1237.8	328.33	147.74	40.2	4.92	22	6	44.3
0	0	791.27	1237.8	328.33	147.74	53.6	4.92	22	6	43.7
0	40	749	1333	362	181	0	3.2	0	0	41.9
0	40	749	1333	362	181	2.4	3.2	14	18	40.6
0	40	749	1333	362	181	4.8	3.2	14	18	44.7
0	40	749	1333	362	181	7.2	3.2	14	18	42.1
56	0	770	350	560	170	0	5.6	0	0	24.53
56	0	770	350	560	170	11.2	5.6	28	23	26.37
56	0	770	350	560	170	22.4	5.6	28	23	27.5
56	0	770	350	560	170	33.6	5.6	28	23	28.76
56	0	770	350	560	170	44.8	5.6	28	23	27.66

Dataset parameters for compressive strength of GFC (continued)

MicroSilica (Kg/m^3)	Fly Ash (Kg/m^3)	Fine aggregate (Kg/m^3)	Coarse aggregate (Kg/m^3)	Cement (Kg/m^3)	Water (Kg/m^3)	Amount of fibre (Kg/m^3)	SP (Kg/m^3)	Diameter (μm)	Length (mm)	Compressive strength (MPa)
0	0	845	880	390	221.38	0	0	0	0	38.94
0	0	845	880	390	221.38	6.5	0.45	14	12	42.71
0	0	845	880	390	221.38	13	0.98	15	12	42.26
0	0	845	880	390	221.38	19.5	2.13	16	12	41.46
132	0	940	0	940	319.6	0	3.4	0	0	40
132	0	940	0	940	319.6	7	3.4	14	20	50.21
132	0	940	0	940	319.6	21	3.4	14	20	55.83
132	0	940	0	940	319.6	35	3.4	14	20	59.17
0	0	900	650	450	190	0	5	0	0	71.26
0	0	900	650	450	190	2.68	5.12	14	12	70.4
0	0	900	650	450	190	5.36	5.15	14	12	70
0	0	900	650	450	190	8.04	5.4	14	12	68.45
0	0	900	650	450	190	10.72	5.65	14	12	67.377
0	0	900	650	450	190	13.4	5.85	14	12	63.836
0	0	900	650	450	190	16.08	6	14	12	60.662
0	0	900	650	450	190	18.76	6.15	14	12	53.36
0	0	900	650	450	190	21.44	6.25	14	12	47.606
0	0	865	1075	335	182	0	0	0	0	34.597
0	0	862	1072	335	182	6.5	0.56	14	12	35.169
0	0	859	1069	335	182	13	1.4	14	12	36.838
0	0	852	1062	335	182	26	2.35	14	12	35.468
0	137.5	768.5	768.6	412.5	192.5	0	5.5	0	0	71.767
0	137.5	768.5	768.6	412.5	192.5	9.1	6.05	13	12	70.882
0	137.5	768.5	768.6	412.5	192.5	18.2	7.15	13	12	70.503
0	137.5	768.5	768.6	412.5	192.5	26	7.69	13	12	73.157
0	137.5	768.5	768.6	412.5	192.5	39	8.79	13	12	74.548
11	137.5	766.6	766.6	401.5	192.5	0	7.14	0	0	74.522
11	137.5	766.6	766.6	401.5	192.5	9.1	12.08	13	12	74.169
11	137.5	766.6	766.6	401.5	192.5	18.2	13.18	13	12	74.421
11	137.5	766.6	766.6	401.5	192.5	26	14.28	13	12	74.978
11	137.5	766.6	766.6	401.5	192.5	39	15.93	13	12	78.163
22	137.5	764.7	764.8	390.5	192.5	0	20.88	0	0	77.733
22	137.5	764.7	764.8	390.5	192.5	9.1	21.99	13	12	78.656
22	137.5	764.7	764.8	390.5	192.5	18.2	23.62	13	12	80.919
22	137.5	764.7	764.8	390.5	192.5	26	24.72	13	12	81.323
22	137.5	764.7	764.8	390.5	192.5	39	26.37	13	12	84.079
0	0	751.319	1010.35	450	162	0	0	0	0	47.77
0	0	751.319	1010.35	450	162	0.54	0	13	6	50.19
0	0	751.319	1010.35	450	162	0.81	0	13	6	53.66
0	0	751.319	1010.35	450	162	1.08	0	13	6	57.33
0	133.19	853.1	782.6	430	154.8	0	4.5	0	0	54.44
0	133.19	853.1	782.6	430	154.8	0.54	4.5	13	6	57.55
0	133.19	853.1	782.6	430	154.8	0.81	4.5	13	6	61.33
0	133.19	853.1	782.6	430	154.8	1.08	4.5	13	6	65.55
0	0	752	1158	440	176	0	0	0	0	29.973
0	0	752	1158	440	176	3.3	0	14	12	29.633
0	0	752	1158	440	176	5.808	0	14	12	23.2
0	0	752	1158	440	176	11.572	0	14	12	26.327

Appendix C

Dataset parameters for split tensile strength of GFC

MicroSilica (Kg/m^3)	Fly Ash (Kg/m^3)	Fine aggregate (Kg/m^3)	Coarse aggregate (Kg/m^3)	Cement (Kg/m^3)	Water (Kg/m^3)	Amount of fibre (Kg/m^3)	SP (Kg/m^3)	Diameter (μm)	Length (mm)	Split-tensile strength (MPa)
0	0	680	1225	440	157	0	0	0	0	4.278
0	0	680	1225	440	157	2.4	0	12	50	4.351
0	0	680	1225	440	157	3.2	0	12	50	4.4732
0	0	680	1225	440	157	4	0	12	50	4.635
0	0	680	1225	440	157	4.8	0	12	50	4.808
0	0	680	1225	440	157	2.4	0	14	15	4.523
0	0	680	1225	440	157	3.2	0	14	15	4.685
0	0	680	1225	440	157	4	0	14	15	4.857
0	0	680	1225	440	157	4.8	0	14	15	4.908
0	0	1100	740	350	175	0	3.5	0	0	3.659

Dataset parameters for split tensile strength of GFC (continued)

MicroSilica (Kg/m^3)	Fly Ash (Kg/m^3)	Fine aggregate (Kg/m^3)	Coarse aggregate (Kg/m^3)	Cement (Kg/m^3)	Water (Kg/m^3)	Amount of fibre (Kg/m^3)	SP (Kg/m^3)	Diameter (μm)	Length (mm)	Split-tensile strength (MPa)
0	0	1100	740	350	175	0.5	3.5	18.5	24	3.805
0	0	1100	740	350	175	1	3.5	18.5	24	4
0	0	1100	740	350	175	2	3.5	18.5	24	3.861
0	0	1100	740	350	175	3	3.5	18.5	24	3.625
0	0	765	935	400	200	0	0	0	0	3.03
0	0	765	935	400	200	6.25	0	14	12	3.61
26.5	0	740	890	503.5	195	1.007	10.07	14	12	6.55
26.5	0	740	890	503.5	195	2.014	10.07	14	12	6.82
26.5	0	740	890	503.5	195	3.021	10.07	14	12	7.01
26.5	0	740	890	503.5	195	4.028	10.07	14	12	6.54
0	0	825	980	355	195	0	0	0	0	2.781
0	0	825	980	355	195	6.5	0.89	14	12	3.3
0	0	825	980	355	195	13	1.45	14	12	3.373
0	0	825	980	355	195	19.5	2.31	14	12	3.365
0	0	825	980	355	195	26	2.84	14	12	3.277
22	86	655	1165	280	129	0	6.45	0	0	7.18
22	86	655	1165	280	129	10.62	6.45	15	12	7.69
22	86	655	1165	280	129	21.24	6.45	15	12	9.2
22	86	655	1165	280	129	30.68	6.45	15	12	10.01
55	0	600	950	550	143	0	18	0	0	4.99
55	0	600	950	550	143	13	18	14	36	5.15
55	0	600	950	550	143	19.5	18	14	36	5.43
55	0	600	950	550	143	26	18	14	36	5.67
55	0	600	950	550	143	32.5	18	14	36	5.87
55	0	600	950	550	143	39	18	14	36	5.76
55	0	600	950	550	143	45.5	18	14	36	5.43
55	0	600	950	550	143	52	18	14	36	5.29
0	0	791.27	1237.8	328.33	147.74	26.8	4.92	22	6	4.8
0	40	749	1333	362	181	0	3.2	0	0	3.74
0	40	749	1333	362	181	2.4	3.2	14	18	3.75
0	40	749	1333	362	181	4.8	3.2	14	18	4.41
0	40	749	1333	362	181	7.2	3.2	14	18	3.78
56	0	770	350	560	170	0	5.6	0	0	2.09
56	0	770	350	560	170	11.2	5.6	28	23	3.03
56	0	770	350	560	170	22.4	5.6	28	23	4.13
56	0	770	350	560	170	33.6	5.6	28	23	5.33
56	0	770	350	560	170	44.8	5.6	28	23	4.24
0	0	845	880	390	221.38	0	0	0	0	3.14
0	0	845	880	390	221.38	6.5	0.45	14	12	3.57
0	0	845	880	390	221.38	13	0.98	15	12	3.71
0	0	845	880	390	221.38	19.5	2.13	16	12	3.65
0	0	900	650	450	190	0	5	0	0	5.741
0	0	900	650	450	190	2.68	5.12	14	12	5.852
0	0	900	650	450	190	5.36	5.15	14	12	5.981
0	0	900	650	450	190	8.04	5.4	14	12	6.089
0	0	900	650	450	190	10.72	5.65	14	12	6.263
0	0	900	650	450	190	13.4	5.85	14	12	6.350
0	0	900	650	450	190	16.08	6	14	12	6.566
0	0	900	650	450	190	18.76	6.15	14	12	6.678
0	0	900	650	450	190	21.44	6.25	14	12	6.695
0	137.5	768.5	768.6	412.5	192.5	0	5.5	0	0	3.101
0	137.5	768.5	768.6	412.5	192.5	9.1	6.05	13	12	3.249
0	137.5	768.5	768.6	412.5	192.5	18.2	7.15	13	12	3.402
0	137.5	768.5	768.6	412.5	192.5	26	7.69	13	12	3.649
0	137.5	768.5	768.6	412.5	192.5	39	8.79	13	12	3.901
11	137.5	766.6	766.6	401.5	192.5	0	7.14	0	0	3.249
11	137.5	766.6	766.6	401.5	192.5	9.1	12.08	13	12	3.515
11	137.5	766.6	766.6	401.5	192.5	18.2	13.18	13	12	3.697
11	137.5	766.6	766.6	401.5	192.5	26	14.28	13	12	3.818
11	137.5	766.6	766.6	401.5	192.5	39	15.93	13	12	4.047
22	137.5	764.7	764.8	390.5	192.5	0	20.88	0	0	3.58
22	137.5	764.7	764.8	390.5	192.5	9.1	21.99	13	12	3.69
22	137.5	764.7	764.8	390.5	192.5	18.2	23.62	13	12	3.951
22	137.5	764.7	764.8	390.5	192.5	26	24.72	13	12	4.153
22	137.5	764.7	764.8	390.5	192.5	39	26.37	13	12	4.387
0	0	751.319	1010.35	450	162	0	0	0	0	3.6
0	0	751.319	1010.35	450	162	0.54	0	13	6	3.78

Dataset parameters for split tensile strength of GFC (continued)

MicroSilica (Kg/m^3)	Fly Ash (Kg/m^3)	Fine aggregate (Kg/m^3)	Coarse aggregate (Kg/m^3)	Cement (Kg/m^3)	Water (Kg/m^3)	Amount of fibre (Kg/m^3)	SP (Kg/m^3)	Diameter (μm)	Length (mm)	Split-tensile strength (MPa)
0	0	751.319	1010.35	450	162	0.81	0	13	6	3.92
0	0	751.319	1010.35	450	162	1.08	0	13	6	4.1
0	133.19	853.1	782.6	430	154.8	0	4.5	0	0	3.85
0	133.19	853.1	782.6	430	154.8	0.54	4.5	13	6	4.13
0	133.19	853.1	782.6	430	154.8	0.81	4.5	13	6	4.24
0	133.19	853.1	782.6	430	154.8	1.08	4.5	13	6	4.39
0	0	752	1158	440	176	0	0	0	0	2
0	0	752	1158	440	176	3.3	0	14	12	2.1
0	0	752	1158	440	176	5.808	0	14	12	3.41
0	0	752	1158	440	176	11.572	0	14	12	3.07

Data Availability

Data will be made available on request.

References

[1] S. Sbahieh, M. Rabie, U. Ebead, S.G. Al-Ghamdi, The mechanical and environmental performance of fiber-reinforced polymers in concrete structures: opportunities, challenges and future directions, Buildings 12 (2022) 1417.

[2] M.S. Saif, A.S. Shanour, G.E. Abdelaziz, H.I. Elsayad, I.G. Shaaban, B.A. Tayeh, M. S. Hammad, Influence of blended powders on properties of ultra-high strength fibre reinforced self compacting concrete subjected to elevated temperatures, Case Stud. Constr. Mater. 18 (2023) e01793.

[3] M.R. Irshidat, N. Al-Nuaimi, M. Rabie, Hybrid effect of carbon nanotubes and polypropylene microfibers on fire resistance, thermal characteristics and microstructure of cementitious composites, Constr. Build. Mater. 266 (2021) 121154.

[4] A.S. Fayed, A.S. Sherbini, H.S.S. Abou El-Mal, Mixed mode fracture behavior of fiber reinforced concrete; experimental and numerical analysis adopting cracked Brazilian disc specimen, Ain Shams Eng. J. 14 (2023) 102132, https://doi.org/10.1016/j.asej.2023.102132.

[5] A. Ulu, A.I. Tutar, A. Kurklu, F. Cakir, Effect of excessive fiber reinforcement on mechanical properties of chopped glass fiber reinforced polymer concretes, Constr. Build. Mater. 359 (2022) 129486, https://doi.org/10.1016/j.conbuildmat.2022.129486.

[6] M.S. Khan, A. Fuzail Hashmi, M. Shariq, S.M. Ibrahim, Effects of incorporating fibres on mechanical properties of fibre-reinforced concrete: a review, Mater. Today Proc. (2023), https://doi.org/10.1016/j.matpr.2023.05.106.

[7] Y. Ju, M. Zhu, X. Zhang, D. Wang, Influence of steel fiber and polyvinyl alcohol fiber on properties of high performance concrete, Struct. Concr. 23 (2022) 1687–1703, https://doi.org/10.1002/suco.202100775.

[8] J. Yu, Y. Chen, C. Leung, Mechanical performance of Strain-Hardening Cementitious Composites (SHCC) with hybrid polyvinyl alcohol and steel fibers, Compos. Struct. (2019), https://doi.org/10.1016/J.COMPSTRUCT.2019.111198.

[9] P. Zhang, Y. Zheng, K. Wang, K. Zhang, Combined influence of nano-CaCO3 and polyvinyl alcohol fibers on fresh and mechanical performance of concrete incorporating fly ash, Struct. Concr. 21 (2019) 724–734, https://doi.org/10.1002/suco.201900134.

[10] V. Sivakumar, O. Kavitha, G. Arulraj, V. Srisanthi, An experimental study on combined effects of glass fiber and Metakaolin on the rheological, mechanical, and durability properties of self-compacting concrete, Appl. Clay Sci. 147 (2017) 123–127, https://doi.org/10.1016/J.CLAY.2017.07.015.

[11] M. Madhkhan, R. Katirai, Effect of pozzolanic materials on mechanical properties and aging of glass fiber reinforced concrete, Constr. Build. Mater. (2019), https://doi.org/10.1016/J.CONBUILDMAT.2019.07.128.

[12] Y. Ju, M. Zhu, X. Zhang, D. Wang, Influence of steel fiber and polyvinyl alcohol fiber on properties of high performance concrete, Struct. Concr. 23 (2022) 1687–1703, https://doi.org/10.1002/suco.202100775.

[13] Z. Yuan, Y. Jia, Mechanical properties and microstructure of glass fiber and polypropylene fiber reinforced concrete: an experimental study, Constr. Build. Mater. 266 (2021) 121048, https://doi.org/10.1016/J.CONBUILDMAT.2020.121048.

[14] M. Anjum, K. Khan, W. Ahmad, A. Ahmad, M.N. Amin, A. Nafees, Application of ensemble machine learning methods to estimate the compressive strength of fiber-reinforced nano-silica modified concrete, Polymers 14 (2022) 3906, https://doi.org/10.3390/polym14183906.

[15] Q.-F. Li, Z.-M. Song, High-performance concrete strength prediction based on ensemble learning, Constr. Build. Mater. 324 (2022) 126694.

[16] H. Thiagu, T.C. Madhavi, Optimization of fibre reinforced foam concrete for the mechanical behaviour by artificial neural network, Asian J. Civ. Eng. 24 (2023) 3175–3190.

[17] C. Cs, B.U. Shankar, Effect of foundry sand and glass fibres in concrete using artificial neural network, J. Civ. Eng. 11 (2020).

[18] G. Nakkeeran, L. Krishnaraj, A. Bahrami, H. Almujibah, H. Panchal, M.M.A. Zahra, Machine learning application to predict the mechanical properties of glass fiber mortar, Adv. Eng. Softw. 180 (2023) 103454, https://doi.org/10.1016/j.advengsoft.2023.103454.

[19] Travis Perkins | Builders' Merchant | Building Supplies, (n.d.). ⟨https://www.travisperkins.co.uk/⟩ (accessed June 20, 2024).

[20] B. Ali, L.A. Qureshi, Influence of glass fibers on mechanical and durability performance of concrete with recycled aggregates, Constr. Build. Mater. 228 (2019) 116783, https://doi.org/10.1016/j.conbuildmat.2019.116783.

[21] BS EN 12350–2:2019 - TC. Testing fresh concrete. Slump-test, British Standards Institution, London, UK, 2019..

[22] BS 1881: Part 116:1983. Testing concrete. Method for determination of compressive strength of concrete cubes, British Standards Institution, London, UK, 1983..

[23] ASTM C496/C496M-17, Standard Test Method for Splitting Tensile Strength of Cylindrical Concrete Specimens, ASTM International, West Conshohocken, PA, 2017..

[24] J. Sanjeev, K.J.N. Sai Nitesh, Study on the effect of steel and glass fibers on fresh and hardened properties of vibrated concrete and self-compacting concrete, Mater. Today Proc. 27 (2020) 1559–1568, https://doi.org/10.1016/j.matpr.2020.03.208.

[25] Y.R. Atewi, M.F. Hasan, E. Güneyisi, Fracture and permeability properties of glass fiber reinforced self-compacting concrete with and without nanosilica, Constr. Build. Mater. 226 (2019) 993–1005, https://doi.org/10.1016/j.conbuildmat.2019.08.029.

[26] B. Ali, L.A. Qureshi, S.U. Khan, Flexural behavior of glass fiber-reinforced recycled aggregate concrete and its impact on the cost and carbon footprint of concrete pavement, Constr. Build. Mater. 262 (2020) 120820, https://doi.org/10.1016/j.conbuildmat.2020.120820.

[27] V.R. Sivakumar, O.R. Kavitha, G. Prince Arulraj, V.G. Srisanthi, An experimental study on combined effects of glass fiber and Metakaolin on the rheological, mechanical, and durability properties of self-compacting concrete, Appl. Clay Sci. 147 (2017) 123–127, https://doi.org/10.1016/j.clay.2017.07.015.

[28] P. Asokan, M. Osmani, A. Price, Improvement of the mechanical properties of glass fibre reinforced plastic waste powder filled concrete, Constr. Build. Mater. 24 (2010) 448–460, https://doi.org/10.1016/j.conbuildmat.2009.10.017.

[29] M. Mastali, A. Dalvand, A.R. Sattarifard, The impact resistance and mechanical properties of reinforced self-compacting concrete with recycled glass fibre reinforced polymers, J. Clean. Prod. 124 (2016) 312–324, https://doi.org/10.1016/j.jclepro.2016.02.148.

[30] A.K. Parashar, A. Gupta, Investigation of the effect of bagasse ash, hooked steel fibers and glass fibers on the mechanical properties of concrete, Mater. Today Proc. 44 (2021) 801–807, https://doi.org/10.1016/j.matpr.2020.10.711.

[31] L. Qureshi, A. Raza, S. Rehman, M. Nawaz, M. Rashid, Influence of glass fibers on mechanical properties of concrete with recycled coarse aggregates, Civ. Eng. J. 5 (2019) 1007–1019, https://doi.org/10.28991/cej-2019-03091307.

[32] J. Ahmad, R.A. González-Lezcano, A. Majdi, N. Ben Kahla, A.F. Deifalla, M.A. El-Shorbagy, Glass fibers reinforced concrete: overview on mechanical, durability and microstructure analysis, Materials 15 (2022) 5111, https://doi.org/10.3390/ma15155111.

[33] J. Ahmad, O. Zaid, F. Aslam, M. Shahzaib, R. Ullah, H. Alabduljabbar, K. M. Khedher, A study on the mechanical characteristics of glass and nylon fiber reinforced peach shell lightweight concrete, Materials 14 (2021) 4488, https://doi.org/10.3390/ma14164488.

[34] L. Hou, B. Wen, W. Huang, X. Zhang, X. Zhang, Mechanical properties and microstructure of polypropylene–glass-fiber-reinforced desert sand concrete, Polymers 15 (2023) 4675, https://doi.org/10.3390/polym15244675.

[35] H. Tahir, M.B. Khan, N. Shafiq, D. Radu, M.H. Nyarko, A. Waqar, H.R. Almujibah, O. Benjeddou, Optimisation of mechanical characteristics of alkali-resistant glass fibre concrete towards sustainable construction, Sustainability 15 (2023), https://doi.org/10.3390/su151411147.

[36] A. Singh, A. Charak, K.P. Biligiri, V. Pandurangan, Glass and carbon fiber reinforced polymer composite wastes in pervious concrete: material characterization and lifecycle assessment, Resour. Conserv. Recycl 182 (2022) 106304, https://doi.org/10.1016/j.resconrec.2022.106304.

[37] T. Jeevetha, S. VijayaShanthy, A. Sivakumar, N.B. Singh, Evaluation on strength parameters of self-compacting concrete incorporated with carbon and glass fibres,

Mater. Today Proc. 45 (2021) 708–712, https://doi.org/10.1016/j.matpr.2020.02.743.
[38] B. Ali, L.A. Qureshi, Influence of glass fibers on mechanical and durability performance of concrete with recycled aggregates, Constr. Build. Mater. 228 (2019) 116783, https://doi.org/10.1016/j.conbuildmat.2019.116783.
[39] M. Madhkhan, R. Katirai, Effect of pozzolanic materials on mechanical properties and aging of glass fiber reinforced concrete, Constr. Build. Mater. 225 (2019) 146–158, https://doi.org/10.1016/j.conbuildmat.2019.07.128.
[40] M. Abdi Moghadam, R.A. Izadifard, Effects of steel and glass fibers on mechanical and durability properties of concrete exposed to high temperatures, Fire Saf. J. 113 (2020) 102978, https://doi.org/10.1016/j.firesaf.2020.102978.
[41] J.K. Ganta, M.V. Seshagiri Rao, S.S. Mousavi, V. Srinivasa Reddy, C. Bhojaraju, Hybrid steel/glass fiber-reinforced self-consolidating concrete considering packing factor: mechanical and durability characteristics, Structures 28 (2020) 956–972, https://doi.org/10.1016/j.istruc.2020.09.042.
[42] Z. Yuan, Y. Jia, Mechanical properties and microstructure of glass fiber and polypropylene fiber reinforced concrete: an experimental study, Constr. Build. Mater. 266 (2021) 121048, https://doi.org/10.1016/j.conbuildmat.2020.121048.
[43] S.T. Tassew, A.S. Lubell, Mechanical properties of glass fiber reinforced ceramic concrete, Constr. Build. Mater. 51 (2014) 215–224, https://doi.org/10.1016/j.conbuildmat.2013.10.046.
[44] F. Cakir, Evaluation of mechanical properties of chopped glass/basalt fibers reinforced polymer mortars, Case Stud. Constr. Mater. 15 (2021) e00612, https://doi.org/10.1016/j.cscm.2021.e00612.
[45] M.E. Arslan, Effects of basalt and glass chopped fibers addition on fracture energy and mechanical properties of ordinary concrete: CMOD measurement, Constr. Build. Mater. 114 (2016) 383–391, https://doi.org/10.1016/j.conbuildmat.2016.03.176.
[46] A. Tibebu, E. Mekonnen, L. Kumar, J. Chimdi, H. Hailu, N. Fikadu, Compression and workability behavior of chopped glass fiber reinforced concrete, Mater. Today Proc. 62 (2022) 5087–5094, https://doi.org/10.1016/j.matpr.2022.02.427.
[47] T. Thaker, S.P. Dalal, R. Motiani, H. Contractor, Effect of electrical grade glass fibers and alkaline resistant glass fibers on high strength concrete, Mater. Today Proc. 62 (2022) 6998–7001, https://doi.org/10.1016/j.matpr.2021.12.542.
[48] H. Alguhi, D. Tomlinson, Experimental and analytical study of steel and chopped glass fibre reinforced concrete under compression, Constr. Build. Mater. 418 (2024) 135421, https://doi.org/10.1016/j.conbuildmat.2024.135421.
[49] M. Waskom, seaborn: statistical data visualization, J. Open Source Softw. 6 (2021) 3021, https://doi.org/10.21105/JOSS.03021.
[50] M. Jalal, P. Arabali, Z. Grasley, J.W. Bullard, H. Jalal, Behavior assessment, regression analysis and support vector machine (SVM) modeling of waste tire rubberized concrete, J. Clean. Prod. 273 (2020) 122960, https://doi.org/10.1016/j.jclepro.2020.122960.
[51] M. Pal, S. Deswal, Support vector regression based shear strength modelling of deep beams, Comput. Struct. 89 (2011) 1430–1439, https://doi.org/10.1016/j.compstruc.2011.03.005.
[52] C. Cortes, V. Vapnik, Support-vector networks, Mach. Learn 20 (1992) 273–297, https://doi.org/10.1109/64.163674.
[53] C.C. Chang, C.J. Lin, LIBSVM: a library for support vector machines, ACM Trans. Intell. Syst. Technol. 2 (2011), https://doi.org/10.1145/1961189.1961199.
[54] C.J.C. Burges, A tutorial on support vector machines for pattern recognition, Data Min. Knowl. Discov. 2 (1998), https://doi.org/10.1023/A:1009715923555.
[55] H. Drucker, C.J. Burges, L. Kaufman, A. Smola, V. Vapnik, Support vector regression machines, Adv. Neural Inf. Process. Syst. 9 (1996).
[56] L. Breiman, J. Friedman, C.J. Stone, R.A. Olshen, Classification and regression trees, CRC press, 1984.
[57] Y. Freund, L. Mason, The alternating decision tree learning algorithm, Icml (1999) 124–133.
[58] K. Fawagreh, M.M. Gaber, E. Elyan, Random forests: from early developments to recent advancements, Syst. Sci. Control Eng. Open Access J. 2 (2014) 602–609.
[59] L. Breiman, Random forests, Mach. Learn 45 (2001) 5–32.
[60] P. Geurts, D. Ernst, L. Wehenkel, Extremely randomized trees, Mach. Learn 63 (2006) 3–42.
[61] J.H. Friedman, Stochastic gradient boosting, Comput. Stat. Data Anal. 38 (2002) 367–378, https://doi.org/10.1016/S0167-9473(01)00065-2.
[62] M.A. Aladsani, H. Burton, S.A. Abdullah, J.W. Wallace, Explainable machine learning model for predicting drift capacity of reinforced concrete walls, Acids Struct. J. 119 (2022).
[63] C. Cakiroglu, M. Shahjalal, K. Islam, S.M.F. Mahmood, A.H.M.M. Billah, M. L. Nehdi, Explainable ensemble learning data-driven modeling of mechanical properties of fiber-reinforced rubberized recycled aggregate concrete, J. Build. Eng. 76 (2023) 107279, https://doi.org/10.1016/J.JOBE.2023.107279.
[64] T. Akiba, S. Sano, T. Yanase, T. Ohta, M. Koyama, Optuna: A Next-generation Hyperparameter Optimization Framework, in: Proc. 25th ACM SIGKDD Int. Conf. Knowl. Discov. Data Min., 2019.
[65] N. Ruben, C. Venkatesh, C. Durga, M. Chand, Comprehensive study on performance of glass fibers-based concrete, Innov. Infrastruct. Solut. 6 (2021) 1–11, https://doi.org/10.1007/s41062-021-00490-4.
[66] H. Othman, H. Marzouk, M. Sherif, Effects of variations in compressive strength and fibre content on dynamic properties of ultra-high performance fibre-reinforced concrete, Constr. Build. Mater. (2019), https://doi.org/10.1016/J.CONBUILDMAT.2018.11.093.
[67] A. Abrishambaf, M. Pimentel, S. Nunes, Influence of fibre orientation on the tensile behaviour of ultra-high performance fibre reinforced cementitious composites, Cem. Concr. Res. 97 (2017) 28–40, https://doi.org/10.1016/J.CEMCONRES.2017.03.007.
[68] S. Fu, B. Lauke, Effects of fiber length and fiber orientation distributions on the tensile strength of short-fiber-reinforced polymers, Compos. Sci. Technol. 56 (1996) 1179–1190, https://doi.org/10.1016/S0266-3538(96)00072-3.